Microwave Synthesis of Fused Pyrans by Humic Acid Supported Ionic Liquid Catalyst and Their Antimicrobial, Antioxidant, Toxicity Assessment, and Molecular Docking Studies

Muthu Thangaraj,[a] Bibhuti Ranjan,[b] Ramesh Muthusamy,[c] Arul Murugesan,[a] and Robert Moonsamy Gengan[a]*

[a]Department of Chemistry, Faculty of Applied Sciences, Durban University of Technology, Durban 4001, South Africa
[b]Department of Biotechnology and Food Technology, Faculty of Applied Sciences, Durban University of Technology, Durban 4001, South Africa
[c]Department of Pharmaceutical Analysis and Quality Assurance, Omega College of Pharmacy, Edulabad, Ghatkesar, Telangana 501 301, India
*E-mail: genganrm@dut.ac.za
Received June 11, 2018
DOI 10.1002/jhet.3465
Published online 00 Month 2019 in Wiley Online Library (wileyonlinelibrary.com).

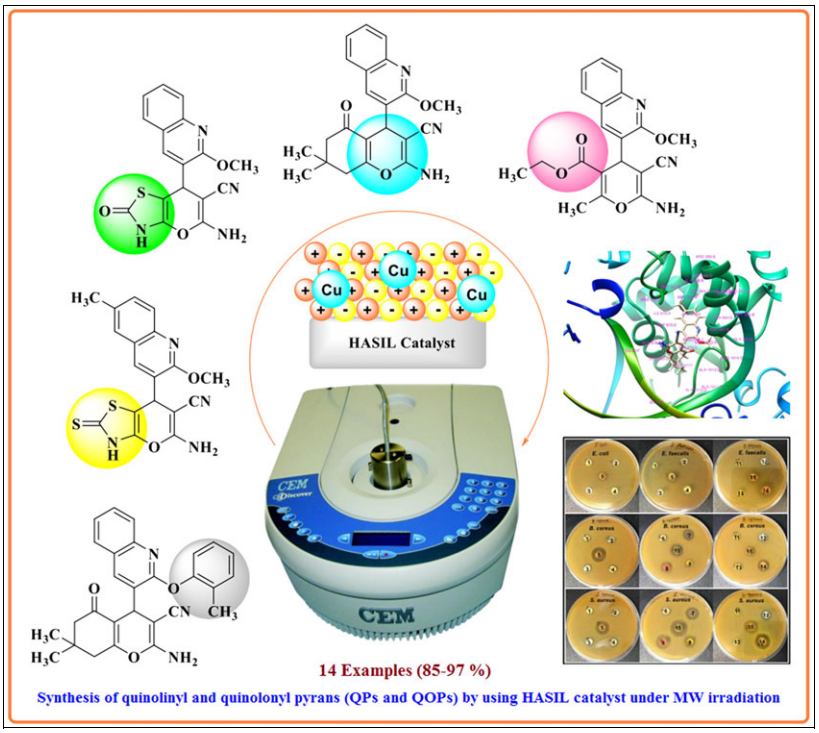

A series of fused quinolinyl and quinolonyl pyrans were synthesized *via* a one-pot reaction of quinolinyl and quinolonyl carbaldehydes, malononitrile, and a 1,3-diketone. The reactions were catalyzed by a new humic acid supported 1-butyl-3-methyl imidazolium thiocyanate ionic liquid under microwave irradiation conditions. Antimicrobial, antioxidant, and toxicity studies displayed various biological activities depending on structure of the pyrans.

J. Heterocyclic Chem., **00,** 00 (2019).

INTRODUCTION

Six-membered heterocyclic compounds containing oxygen, such as pyrans, constitute an important class of natural and synthetic products that plays a fundamental role in bio-organic chemistry and continues to attract research interest [1,2]. The fused pyrans are biologically interesting compounds that display antimicrobial [3], antifungal [4], antitumor [5], anticoagulant, diuretic, spasmolytic, and anti-anaphylactic activities [6–9]. Furthermore, 4*H*-pyrans are building blocks for some important natural products [10,11]. A number of 2-amino-4*H*-pyrans are used as photoactive materials [12], pigments [13], and potentially biodegradable agrochemicals [14]. Because they possess unique pharmacological properties, new methodologies for the synthesis of these compounds have emerged. The simplest synthesis involves a three-component coupling of an aromatic aldehyde, malononitrile, and 1,3-diketones.

Quinoline and its annulated derivatives are highly valuable compounds because of their wide applications as drugs and pharmaceuticals [15,16]. The fused pyran is an important class of compounds that constitute the basic frameworks of a number of alkaloids of biological

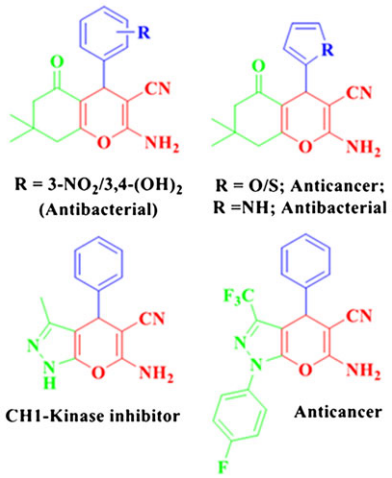

Figure 1. Examples of pyran molecules with biological activities. [Color figure can be viewed at wileyonlinelibrary.com]

significance [17]. Figure 1 shows few examples of fused pyran molecules with biological activities [17]. Therefore, considerable efforts are invested in their synthesis [18] thereby resulting in a large number with important medicinal benefits.

Heterocyclic sulfur-containing molecules have broad application in organic and medicinal chemistry [19]: β-mercapto diketones, as a typical example, display remarkable pharmacological properties such as a diuretic and HIV protease inhibitory [20–23]. Recently, several multicomponent reactions, related to sulfur, have been described [24]. Kornienko and Magedov reported [24] a one-pot synthesis of heterocyclic privileged medicinal scaffolds by using malononitrile with aldehydes and thiols, in ethanol, catalyzed by triethylamine.

During the past two decades, a rapidly growing awareness to environmental issues has catalyzed the thirst for greener and more sustainable technologies in the chemical industry. Ionic liquids (ILs), which consist of cations and anions with low melting points and very low vapor pressures, [25–27] are in great demand as an application in green synthesis. Many different ILs have been prepared and used as solvents and modified catalysts. Homogeneous catalysts in ILs usually provide the advantages of high catalytic activity and good selectivity; however, their widespread usage is associated with some drawbacks such as difficult product isolation and recovery of the catalyst as well as high cost of ILs and their unstudied toxicological properties. Fortunately, ILs in heterogeneous form overcome these drawbacks and moreover, supported solid catalysts with ILs combine the benefits of ILs and heterogeneous catalysis such as good stability of catalytically active species, ease of handling, simple separation, and recycling. In this context, ILs are now widely used for immobilization of homogeneous catalysts [28–31].

The cationic parts of most ILs are organic-based moieties such as imidazolium ions, and the anionic parts can be organic or inorganic and include entities such as thiocyanates, humic substances, nitrates, and acetates. The supported ILs phase catalysis concept is based on a classical homogeneous catalyst that is dissolved in a thin film of ILs that is further dispersed over the high internal surface of porous support. In supported ILs phase materials, the dissolved catalyst still acts microscopically as homogeneously dissolved metal complex in its uniform ILs environment while macroscopically dry solid form that can be recycled easily. Humic acid is a typical

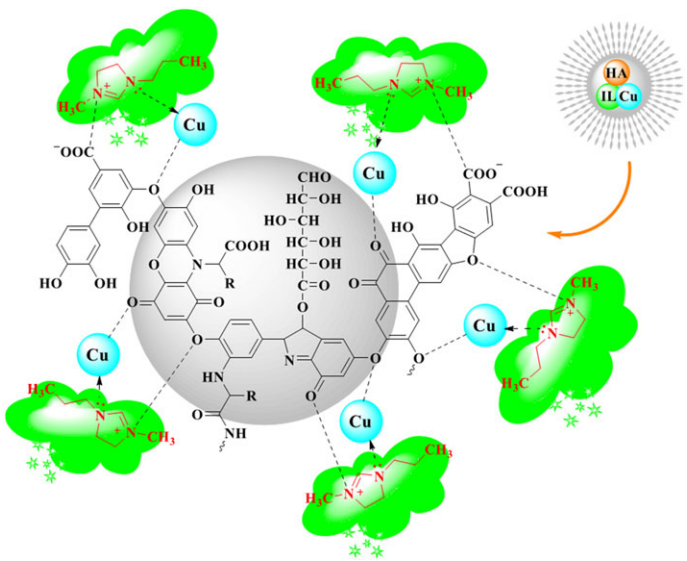

Figure 2. The proposed interaction of HASIL. HASIL, humic acid supported 1-butyl-3-methyl imidazolium thiocyanate. [Color figure can be viewed at wileyonlinelibrary.com]

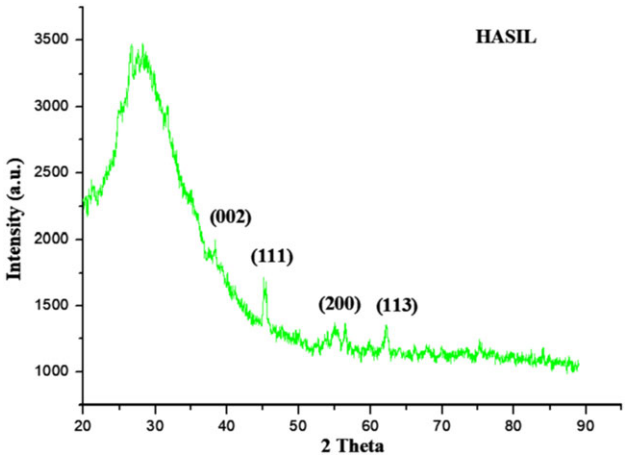

Figure 3. The powder X-Ray Diffraction pattern for HASIL. HASIL, humic acid supported 1-butyl-3-methyl imidazolium thiocyanate. [Color figure can be viewed at wileyonlinelibrary.com]

support material that catalyzes several reactions [32]: it enhances the basic nature of the catalyst and provides a heterogenic system. Heterogeneous catalytic systems display advantages including larger interfacial reaction area, ease of product separation, cost-effectiveness, recyclability, and environmental friendliness.

In this study, humic acid (HA) supported 1-butyl-3-methyl imidazolium thiocyanate (HASIL) catalyst is used for the synthesis of novel fused quinoline and quinolonyl pyrans.

RESULTS AND DISCUSSION

Firstly, a new HASIL material was synthesized by stirring an ethanolic mixture of 1-butyl-3-methylimidazolium thiocyanate IL ([bmim]SCN) and HA under inert atmosphere for 10 h followed by reflux. The solvent was removed *in vacuo* to produce an off-white powder that was treated with a solution of HA and copper acetate to produce the catalyst, after work-up of the reaction content. The proposed possible interaction of copper, HA, and [bmim] SCN [33,34] is shown in Figure 2. The synthesized novel catalyst was analyzed using various techniques including powder X-ray diffraction, scanning electron microscopy (SEM), energy dispersive X-ray spectroscopy, transmission electron microscopy, thermogravimetric analysis (TGA), differential scanning calorimetry (DSC), and Fourier-transform infrared spectroscopy (FTIR).

The X-ray diffraction pattern in the 2θ range from 10°C to 70°C of HASIL (Fig. 3) exhibits very small

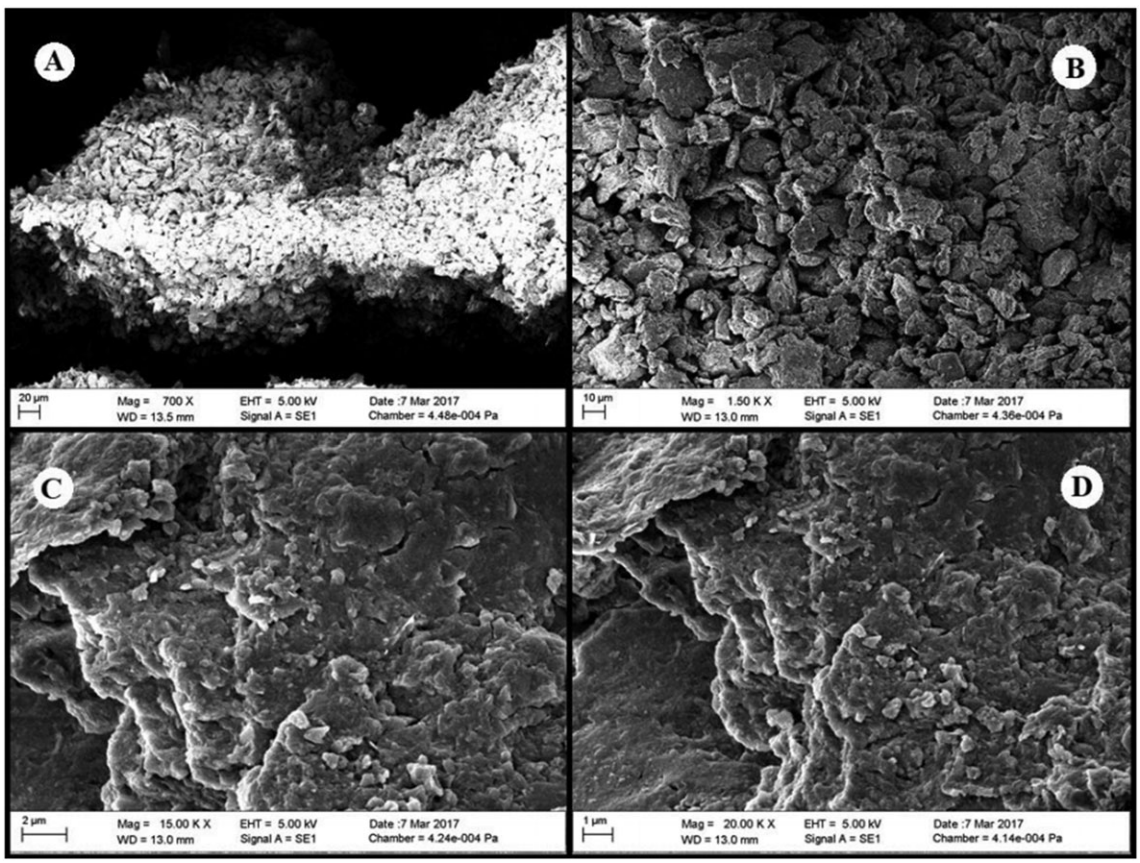

Figure 4. SEM images of the humic acid supported ionic liquid catalyst. SEM, scanning electron microscopy.

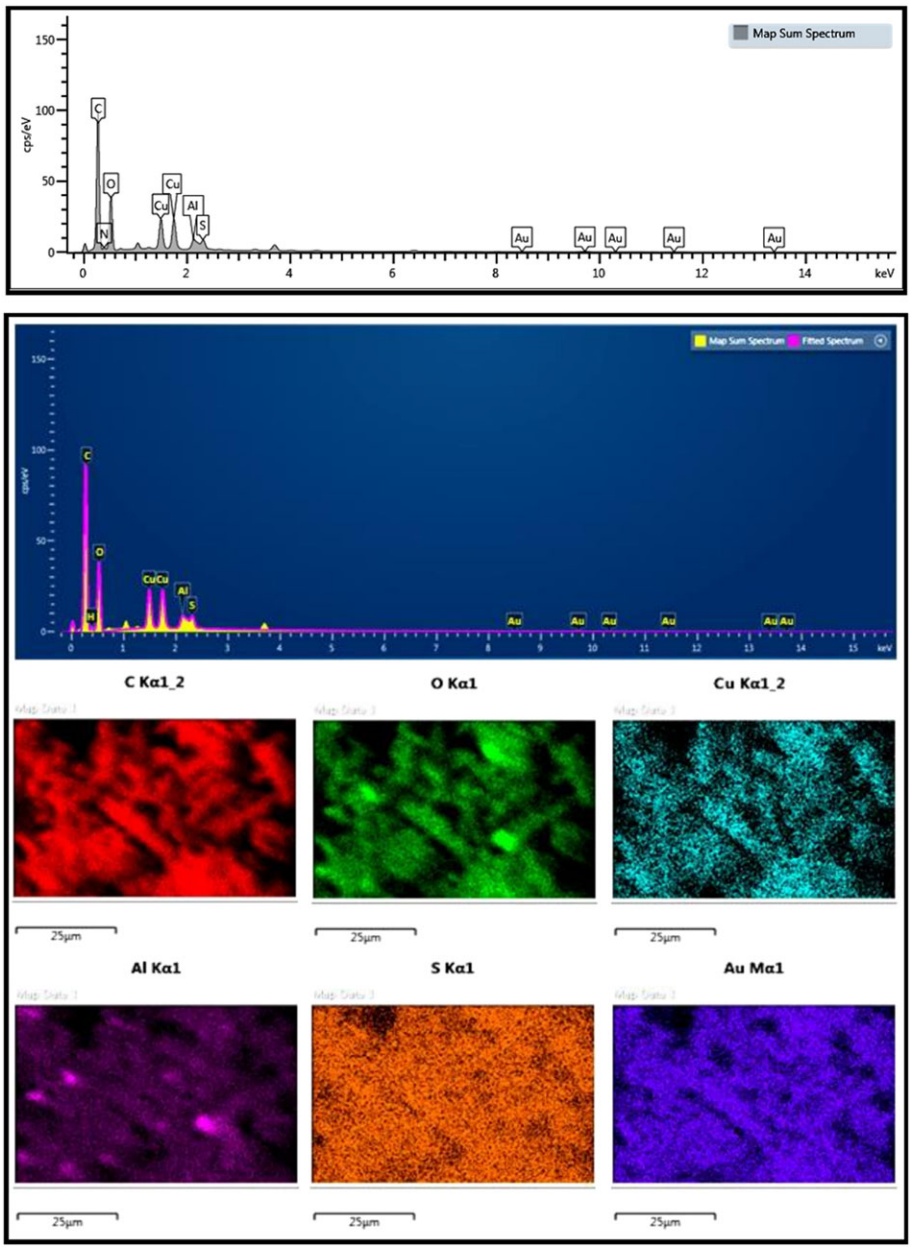

Figure 5. EDX spectra and elemental mapping of HASIL. EDX, energy-dispersive X-ray spectroscopy; HASIL, humic acid supported 1-butyl-3-methyl imidazolium thiocyanate. [Color figure can be viewed at wileyonlinelibrary.com]

diffuse peaks with a few intense peaks, implying its non-crystalline nature. This behavior is consistent with the behavior observed in the case of humic substances from other sources [35,36]. The weaker diffraction lines of HASIL exhibit the humic particles are coated with ILs. The diffraction reflection observed at around 38.5°, 45°, 56°, and 62.5° corresponds to (002), (111), (200), and (113) of Bragg's reflection for cubic structure of copper [37].

Figure 4A, B, C, and D provides the SEM images of HASIL where small particles at 20, 10, 2, and 1 µm are observed. The small particles suggest high metal adsorption [38] is promoted: Cu can form bridges with the carboxyl groups of HA, interact by chemisorption with oxidized carbon atoms, and form coordination compounds [39] with other functional groups of humic substances, such as hydroxyl, phenol, carboxyl, and methoxy functional groups. Compacted microaggregates are found in HASIL. The aggregation phenomenon is important to the transport of metal ions in natural environments [40]. The HA substances in general form thin thread and net-like structures that grow into larger

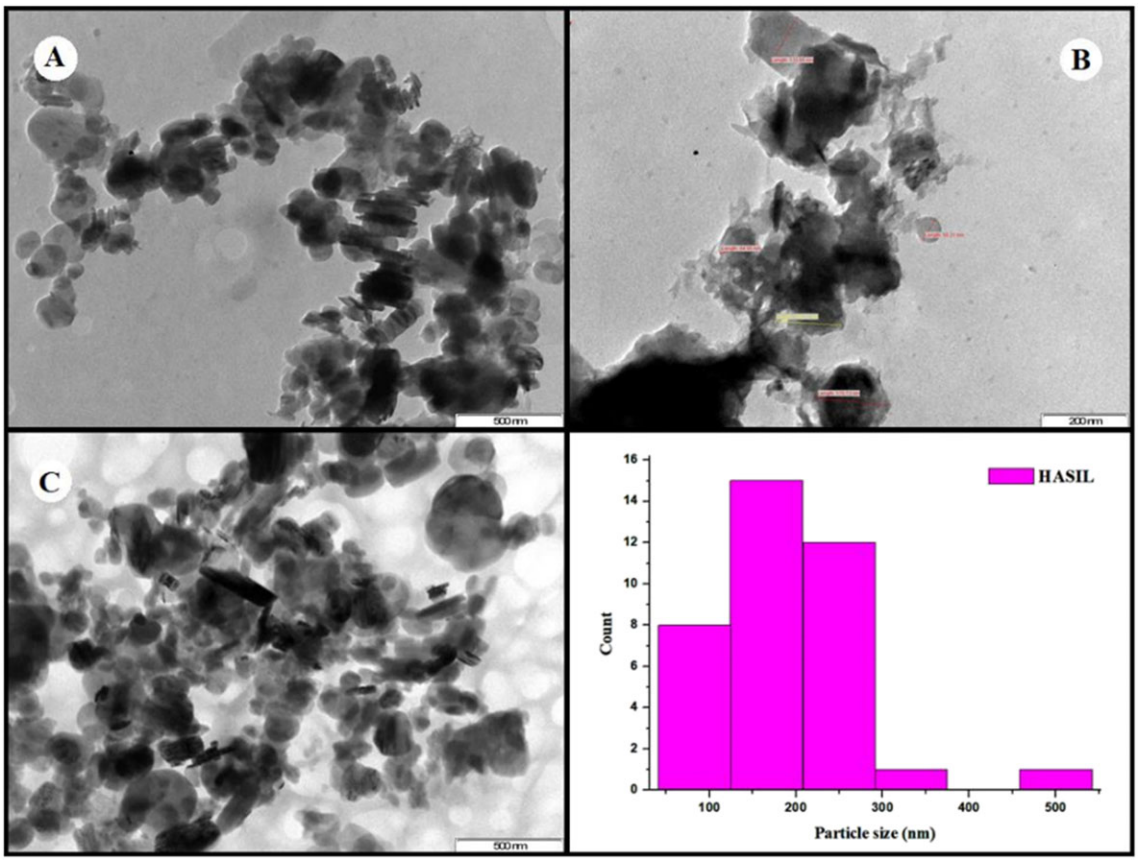

Figure 6. TEM images of HASIL and particle histogram. HASIL, humic acid supported 1-butyl-3-methyl imidazolium thiocyanate; TEM, transmission electron microscopy. [Color figure can be viewed at wileyonlinelibrary.com]

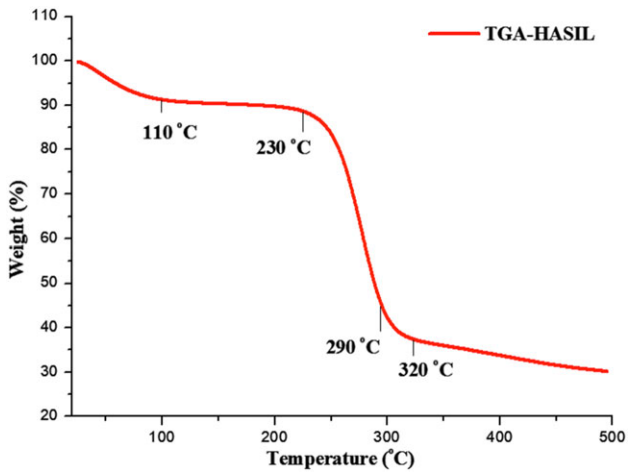

Figure 7. TGA curve of HASIL. HASIL, humic acid supported 1-butyl-3-methyl imidazolium thiocyanate; TGA, thermogravimetric analysis. [Color figure can be viewed at wileyonlinelibrary.com]

rings and sheets with increasing humic and cationic concentrations [41]. The cationic concentrations are because of the IL, [bmim]SCN.

Figure 5 depicts a spectrum acquired from the SEM images of HASIL, revealing the existence of elements such as carbon, oxygen, copper, and gold. The copper peaks were obtained at 1.4 and 1.8 KeV. The elemental mapping is obtained while running Energy-Dispersive X-Ray Spectroscopy spectrum. The appearance of Au peaks is because of the coating of sample with conducting material (Au) to reflect electrons (sputter coating).

The size and morphology of HASIL were obtained by transmission electron microscopy (Fig. 6). The images reveal the formation of maximum number of particles with an average size of 166 nm followed by 250 nm (size variation: ±14 nm calculated by ImageJ, see particle histogram) with an initial process of particle sinterization. The entire HASIL particles contained aggregates with no uniform size and fractal feature. Few of the individual HASIL particles are ellipsoidal in shape (Fig. 6A and C). The smallest particles visible are ~83 nm in size (Fig. 6 histogram).

The TGA curve (Fig. 7) shows that in the temperature range 25°C to 500°C mass losses of HASIL reach about 60% that are most likely caused by destruction of the organic components and condensation of hydroxyl groups at high temperatures [42]. The appearance of a mass loss

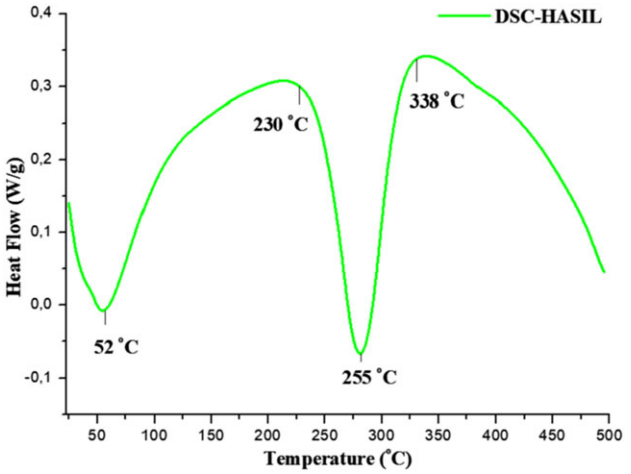

Figure 8. DSC curve of HASIL. DSC, thermogravimetric analysis; HASIL, humic acid supported 1-butyl-3-methyl imidazolium thiocyanate. [Color figure can be viewed at wileyonlinelibrary.com]

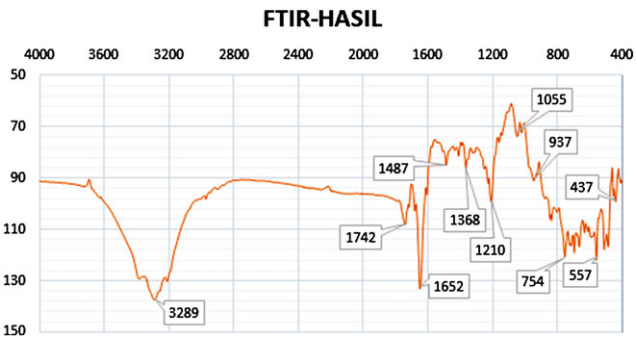

Figure 9. FTIR spectrum of HASIL. FTIR, Fourier-transform infrared; HASIL, humic acid supported 1-butyl-3-methyl imidazolium thiocyanate. [Color figure can be viewed at wileyonlinelibrary.com]

at 110°C is because of the presence of water molecule. As we can see, the main decomposition process starts near 230°C and practically ends to 320°C with a mass loss range 50–60%. The decomposition can be determined by the appearance of ions corresponding to phenolic and carboxylic groups of HA [42]. Almost similar temperature range of 244.6°C to 390.6°C was observed in the literatures for [bmim]SCN that confirmed the strong interaction of IL with HA [43].

The DSC method is convenient for such studies as it is a rapid technique to give characteristic curves, whose variation in enthalpy is associated with phase changes in mineral or soil organic matter, reflecting events related to structures and chemical compositions [44–46]. The areas under the DSC curves were divided into two groups representing different degrees of resistance to thermal oxidation: (a) temperature range (230–338°C), mostly attributable to labile organic matter, mainly compromising phenolic hydrates and other aliphatic compounds. Nevertheless, decarboxylation and dehydration (removal of OH groups during the formation of interaction between HA and [bmim]SCN) should be considered and (b) temperature at 35–175°C, mostly attributable to organic matter, such as polyphenols and polycondensed aromatic substances including HA, humin, and black carbon [47,48]. The following parameters were also determined: temperature of maximum combustion peaks in the DSC curves was observed at 230°C and 338°C with two exothermic peaks and is shown in Figure 8, respectively.

The FTIR spectra (Fig. 9) of HASIL exhibit a strong stretching band at 3289 cm^{-1} that is assigned to the OH stretch of HA. The other absorption observed frequencies (cm^{-1}) at 1210 for C—N, 1652 for C=O, 1487 for C=C, 1055 for —C—O and bending frequencies 1742 for N—H, 1368 for —C—H, and 754 for —CH=CH. The FTIR of HASIL shows absorption bands at 557 cm^{-1} for Cu—O and 437 cm^{-1} for Cu—N. This confirms the formation of —C=N—Cu. A strong stretching vibration band is observed at 937 cm^{-1} for —N—O—Cu. This confirms the formation of —N—O—Cu bond [49]. These results suggest that Cu was adsorbed on the bulk material of HA. The procedure adopted for the preparation of

Scheme 1. Synthesis of 2-methoxy quinoline-3-carbaldehyde and 2-oxo-1,2-dihydropyridine-3-carbaldehyde derivatives [50]. [Color figure can be viewed at wileyonlinelibrary.com]

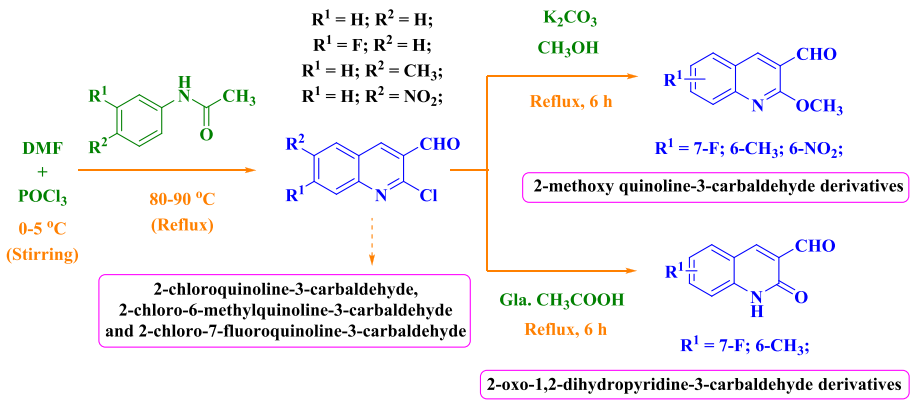

HASIL, where the hydroxyl and carboxylic groups are present in their dissociated form, could create favorable conditions for strong interactions with the positive charges of IL.

After the successful characterization, the HASIL activity was investigated in a one-pot three-component synthesis of quinolinyl pyran derivatives. At first, 2-chloroquinoline-3-carbaldehyde, 2-chloro-6-methylquinoline-3-carbaldehyde, and 2-chloro-7-fluoroquinoline-3-carbaldehyde were synthesized by stirring a mixture of dimethylformamide and $POCl_3$ at 0–5°C followed by refluxing with the corresponding acetanilides at 80–90°C using the Vilsmeier–Haack reaction [50]. Thereafter, the desired starting material 2-methoxy quinoline-3-carbaldehyde was obtained from the reaction of K_2CO_3 with 2-chloroquinoline-3-carbaldehyde in methanol (Scheme 1). The quinolone starting material 2-oxo-1,2-dihydropyridine-3-carbaldehyde derivatives were prepared from the reaction of glacial

Scheme 2. Synthesis of quinolinyl-4*H*-pyrans in the presence of HASIL under microwave irradiation. HASIL, humic acid supported 1-butyl-3-methyl imidazolium thiocyanate. [Color figure can be viewed at wileyonlinelibrary.com]

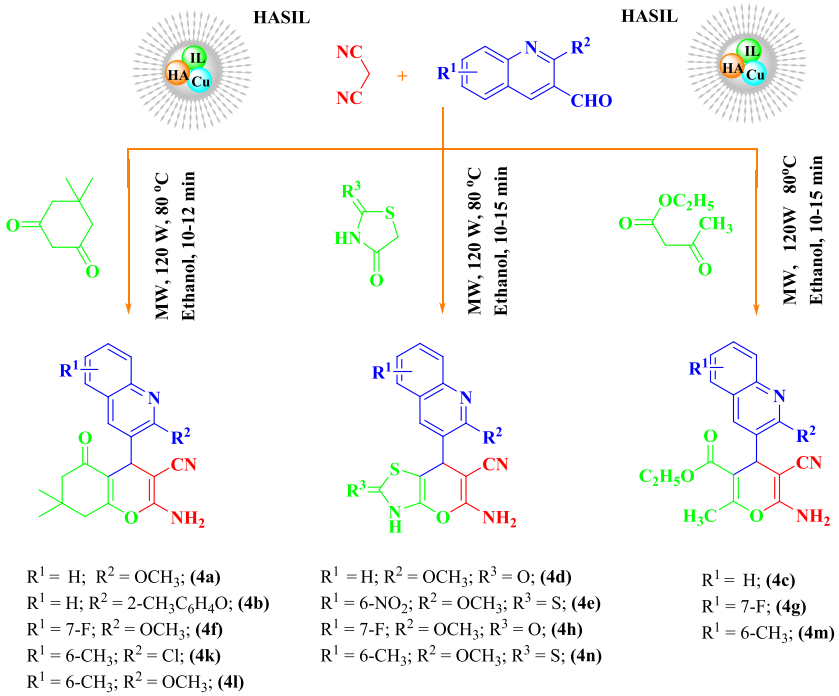

R^1 = H; R^2 = OCH_3; **(4a)**
R^1 = H; R^2 = 2-$CH_3C_6H_4O$; **(4b)**
R^1 = 7-F; R^2 = OCH_3; **(4f)**
R^1 = 6-CH_3; R^2 = Cl; **(4k)**
R^1 = 6-CH_3; R^2 = OCH_3; **(4l)**

R^1 = H; R^2 = OCH_3; R^3 = O; **(4d)**
R^1 = 6-NO_2; R^2 = OCH_3; R^3 = S; **(4e)**
R^1 = 7-F; R^2 = OCH_3; R^3 = O; **(4h)**
R^1 = 6-CH_3; R^2 = OCH_3; R^3 = S; **(4n)**

R^1 = H; **(4c)**
R^1 = 7-F; **(4g)**
R^1 = 6-CH_3; **(4m)**

Scheme 3. Synthesis of quinolonyl-4*H*-pyrans in the presence of HASIL under microwave irradiation (**4i** and **4j**). HASIL, humic acid supported 1-butyl-3-methyl imidazolium thiocyanate. [Color figure can be viewed at wileyonlinelibrary.com]

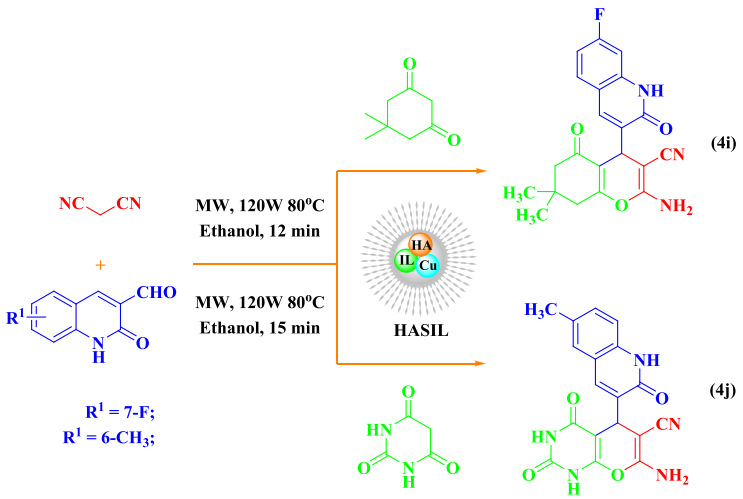

R^1 = 7-F;
R^1 = 6-CH_3;

CH_3COOH with 2-chloro-7-fluoroquinoline-3-carbaldehyde and 2-chloro-6-methylquinoline-3-carbaldehyde.

The three-component reaction was explored from an equivalent mixture of 2-methoxy quinoline-3-carbaldehyde (1 mmol), malononitrile (1 mmol), and dimedone (1 mmol) in the absence of catalyst in ethanol as medium under reflux conditions. Thin-layer chromatography (TLC) was used to monitor the progress of the reaction. There was no products obtained until 24 h.

Thereafter, HASIL was used to carry out the reaction with the same equimolar ratio of the substrates as described earlier. TLC analysis showed a new spot thereby indicating a promising reaction. After 3 h, the mixture was worked-up and the solid was purified by column chromatography using a ethyl acetate : petroleum ether (1:3) solvent system. The obtained yield was 52%. A repeat of the experimental under microwave (MW) irradiation with the power set at 120 W for reaction times of 5, 8, 10, 12, and 15 min, separately, was investigated. A maximum yield of 97% of **4a** was obtained in 10 min. Hence, MW irradiation became the method of choice for the synthesis of new fused quinolinyl and quinolonyl pyrans (Schemes 2 and 3). The structure was confirmed by FTIR, ^{1}H-NMR, ^{13}C-NMR, and elemental analysis.

Fourier-transform infrared, ^{1}H-NMR, and ^{13}C-NMR chemical shifts of quinolinyl pyrans. The FTIR spectrum of **4a** shows stretching frequencies (cm^{-1}) at 2253 for C≡N, 1571 for C═N, 1216 for C─N, 2970 for CH, 1637 for C═C, 1752 for C═O, 2940 for OCH_3, and 3028 for NH. The ^{1}H-NMR spectrum of **4a** showed six singlets for C<u>H</u> (C4′) at δ 4.68, N<u>H</u>$_2$ (C12′) at δ 4.59, methyl proton broad singlet (C<u>H</u>$_3$, C10′) at δ 1.44, broad singlet of (C<u>H</u>$_3$, C9′) at δ 1.05, broad singlet of OC<u>H</u>$_3$ at δ 4.08, and quinolinyl proton singlet C4 at δ 7.91. The dimedone protons (C<u>H</u>$_2$) showed a quartets at δ 2.48 and δ 2.22 for C8′-<u>H</u> and C6′-<u>H</u>, respectively. The ^{13}C-NMR spectrum of **4a** showed the carbonyl group C5′ (C═O) at δ 195.9. The methoxy group C9 (OCH_3) was assigned to δ 53.4. The methyl carbon C9′ at δ 27.0 and C10′ methyl carbon at δ 29.3 were observed. The carbon C6′ (CH_2) showed a peak at δ 50.5, and C8′ showed a peak at δ 40.7. The CH (C4′) carbon showed a peak at δ 32.1, and the carbonitrile CN was observed at δ 111.8. The pyran ring carbon atoms C3′ at δ 60.8 and in the same pyran ring, C2′ at δ 160.1 and C8b′ at δ 158.6, were observed. The dimedone carbonyl carbon C7′ was identified at δ 32.7. The quinolinyl carbon C3 was observed at δ 125.2 and C═N in the quinolinyl ring showed a peak at δ 162.9 and C4 showed a peak at δ 137.8. The selected ^{1}H-NMR and ^{13}C-NMR chemical shifts of **4a** are shown in Figure 10.

The structure was further confirmed on the basis of 2D NMR spectral studies. The ^{13}C, ^{1}H-COSY correlation of carbon signals at δ 137.8, 129.2, 127.6, 126.6, 125.3, 124.0, 53.4, 50.5, 40.7, 32.1, 29.3, and 27.0 were assigned to C4, C7, C5, C8, C6, C4b′, C9, C6′, C8′, C4′, C10′, and C9′, respectively. The carbon signal at δ 137.8 was because of the quinolinyl carbon (C4), and the spectrum is shown in Figure S4.

The ^{1}H, ^{1}H-COSY spectrum of **4a** revealed the correlation between quartet of C6′ (C<u>H</u>$_2$) proton at δ 2.22 and singlet of C<u>H</u>$_3$ (C9′) proton δ 1.05. The C9′ (C<u>H</u>$_3$) proton at δ 1.05 correlated with quartet of C6′ (C<u>H</u>$_2$) proton at δ 2.22 (Fig. S5).

The ^{1}H, ^{1}H-NOESY spectrum revealed the singlet protons (N<u>H</u>$_2$) at δ 4.59 was coupled with a quartet of C6′ (CH_2) at δ 2.22 (Fig. S6).

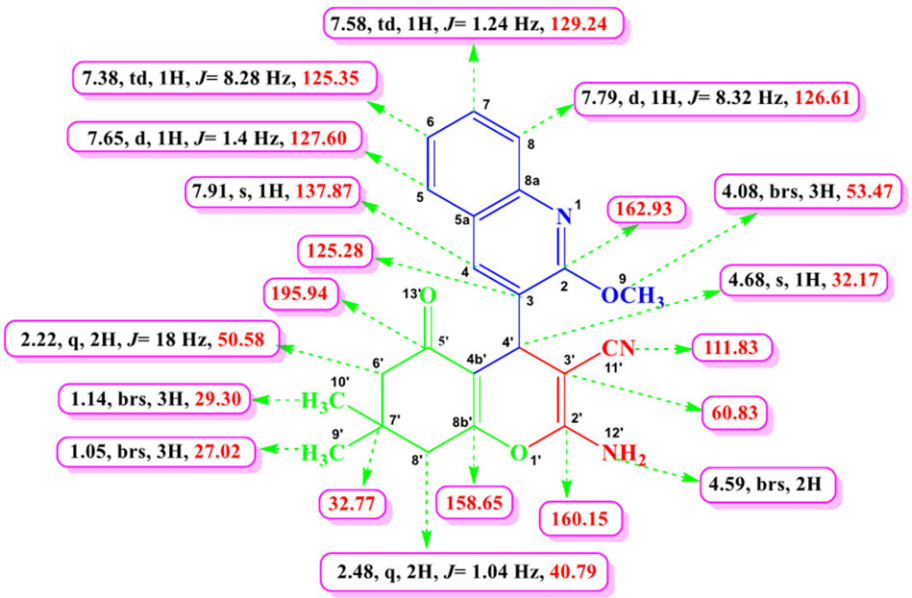

Figure 10. Selected ^{1}H-NMR and ^{13}C-NMR chemical shifts for **4a**. [Color figure can be viewed at wileyonlinelibrary.com]

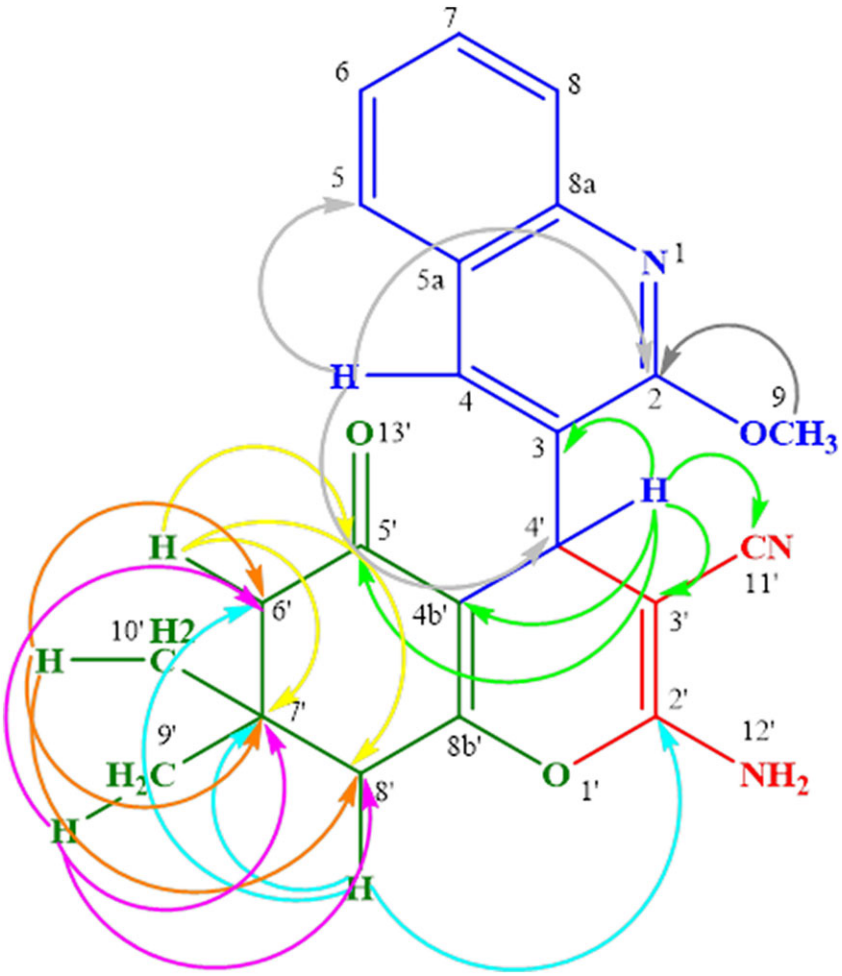

Figure 11. Selected HMBC correlation spectrum of **4a**. HMBC, heteronuclear multiple bond correlation. [Color figure can be viewed at wileyonlinelibrary.com]

Table 1

Selected heteronuclear multiple bond correlations of **4a**.

Entry	Protons	Correlated carbons
1	C4′-H (s, 1H) at δ 4.68 ppm	C3′ (60.83), C11′ (111.83), C3 (125.28), C5′ (195.94), and C4b′ (124.08)
2	C4-H (s, 1H) at δ 7.91 ppm	C4′ (32.17), C5 (127.60), and C2 (163.92)
3	C6′-H (q, 2H) at δ 2.22 ppm	C7′ (32.77), C8′ (40.79), and C5′ (195.94)
4	C8′-H (q, 2H) at δ 2.48 ppm	C7′ (32.77), C6′ (50.58), and C2′ (160.15)
5	C9′-H (brs, 3H) at δ 1.05 ppm	C2 (162.93)
6	C10′-H (brs, 3H) at δ 1.44 ppm	C7′ (32.77), C8′ (40.79), and C6′ (50.58)
7	C4-H (s, 1H) at δ 7.91 ppm	C4′ (32.17), C5 (127.60), and C2 (162.93)

Table 2

Effect of solvents on the synthesis of quinolinyl pyrans[a].

Entry	Solvent	Time (min)	Yield (%)[b]
1	Acetonitrile	15	73
2	Dichloromethane	15	71
3	Ethanol	10	97
4	Methanol	15	88
5	Water	20	35
6	Ethanol–water	15	40

[a]Reaction conditions: aldehyde (1 mmol), malononitrile (1 mmol), 1,3-diketone (1 mmol), and HASIL (10 mol%) were added to the ethanol as solvent (15 mL) under microwave irradiation (120 W) at room temperature.
[b]Isolated yields.

The heteronuclear multiple bond correlation (HMBC) spectrum (Fig. S7) of **4a** shows the long-range correlations as follows: the proton C4′-H (CH) group was coupled with C3′ of pyran ring carbon at δ 60.8 and C11′ carbonitrile CN carbon at δ 111.8, quinolinyl carbon C3 at δ 125.2 and dimedone carbons C5′ at δ 195.9 and C4b′ at δ 124.0.

This correlation of C4′-H to the pyran ring carbon (C3′), carbonitrile carbon (C11′), quaternary carbon (C3) of

Table 3

Effect of optimization of HASIL catalyst.

Entry	Catalyst	Mol %	Time (min)	Yield (%)[a]
1	HA	25	20	Trace
2	HASIL	5	15	71
3	HASIL	10	10	97
4	HASIL	15	15	90
5	HASIL	20	15	90

[a]Isolated yield.

quinoline ring, and carbons C5′ and C4b′ of dimedone indicated that the three groups were attached to C4′ (CH). Thus, it was evident that three different moieties were bonded to a common carbon (C4′) and hence added valuable information to **4a**. The selected ^{1}H-NMR, ^{13}C-NMR, and HMBC chemical shifts are shown in Figure 11.

The C4-H, quinoline proton was coupled with C4′ at δ 32.1, quinolinyl carbons (C5) at δ 127.6, and (C2) at δ 163.9. The C6′-H of dimedone was coupled with C7′ at δ 32.7, C8′ (40.7), and C5′ (195.9). The C8′-H proton was coupled with C7′ at δ 32.7, C6′ (CH_2) at δ 50.5, and C2′ at δ 160.1. The C9′-H (CH_3) was coupled with C2 at δ 162.9. The C10′-H was coupled with C7′ at δ 32.7, C8′ at δ 40.7, and C6′ (CH_2) carbon at δ 50.5. The quinolinyl proton C4-H was coupled with C4′ (CH) carbon at δ 32.1, quinolinyl carbons (C5) at δ 127.6, and C2 at δ 162.9. The selected HMBC correlations of **4a** are shown in Table 1.

Based on the aforementioned spectral details and its elemental analysis (*Anal.* Calcd for $C_{22}H_{21}N_3O_3$: C, 70.38; H, 5.64; N, 11.19; %. Found: C, 70.36; H, 5.65; N, 11.20; %), the structure was confirmed as 2-amino-4-(2-methoxyquinolin-3-yl)-7,7-dimethyl-5-oxo-5,6,7,8-tetrahydro-4*H*-chromene-3-carbonitrile (**4a**).

To determine the effect of solvents and the efficiency of the catalyst, the synthesis of **4a** was selected as model reaction. Solvents such as acetonitrile, DCM, ethanol, ethanol, water, and ethanol–water were used for optimizing the suitable solvent. It was found that ethanol showed a crucial effect on the reaction yield (97%). The yield decreased to 35% when altering the solvents, and the low yield resulted from some unreacted substances (Table 2, entry 5).

When the same substrate mixture was reacted in the presence of HASIL (5 mol %), the isolated yield of **4a** was 71%. In another attempt, a trace amount of product was obtained while HA used as a catalyst (Table 3, entry 1). It was found that in the presence of (10 mol %) HASIL, the yield of **4a** substantially increased to 97% within 10 min (Table 3, entry 3). However, on further increasing the amount of HASIL to 15 mol % and 20 mol %, no improvements in the yield (90%) were observed (Table 3, entries 4 and 5). This shows that the best yield of **4a** was obtained when HASIL is taken at 10 mol %, respectively.

To report the effect of MW irradiation and to evaluate and compare normal refluxing with MW assisted method, various conventional and unconventional conditions were screened. The results are listed in Table 4. Without MW,

Table 4

Effect of microwave (MW) irradiation on the synthesis of quinolinyl pyran[a].

Entry	Power (W)	Time (min)	Yield (%)[b]
1	Without MW (r.t)	24 h	38
2	Without MW (90°C)	3 h	52
3	100	20	75
4	120	10	97
5	150	15	90
6	200	15	90

[a]Reaction conditions: aldehyde (1 mmol), malononitrile (1 mmol), 1,3-diketone (1 mmol), and HASIL (10 mol%) were added to the ethanol as solvent (15 mL).
[b]Isolated yields.

Figure 12. Recyclability of HASIL. HASIL, humic acid supported 1-butyl-3-methyl imidazolium thiocyanate. [Color figure can be viewed at wileyonlinelibrary.com]

Table 5

Effect of optimization of reported catalysts with HASIL catalyst.

Entry	Catalyst	Temp (°C)	Time	Yield (%)	References
1	Montmorillonite K10	125	30 min	96	[57]
2	Fe $(HSO_4)_3$	85	25 min	97	[58]
3	Zwitterionic salt	80	90 min	88	[59]
4	Iodine	125	300 min	87	[60]
5	TCT	100	40 min	95	[61]
6	*p*-TSA	125	240 min	90	[62]
7	$K_5CoW_{12}O_{40}.3H_2O$	125	180 min	78	[63]
8	[FemSILP]-L-Prolinate	100	300 min	87	[64]
9	[TEBSA][HSO_4]	120	10 min	89	[65]
10	[bmim][PF_6]	80	2 h	90	[66]
11	[DMAP-PEG_{1000}-DIL][BF_4]	100	30 min	97	[67]
12	$[PhNMe_2CH_2NMe_2]Cl^-$	80	40 min	95	[68]
13	DABCO	90	2 h	97	[69]
14	$AlCl_3$	110	25 min	52	-
15	CuBr	110	20 min	50	-
16	$ZnCl_2$	110	20 min	53	-
17	B $(OH)_3$	110	25 min	55	-
18	$FeCl_3$	110	30 min	61	-
19	HASIL	80	10 min	97	This work

4a was formed in the presence of HASIL under stirring at room temperature after 24 h. Also the reaction at 90°C and without MW irradiation, the observed yield was 38–52% within 3 h (Table 4, entries 1 and 2). Moreover, the effect of MW irradiation of different powers was investigated. It was observed that the irradiation power of 120 W at 110°C afforded the best yield of **4a**, with 97% isolated yield after 10 min (Table 4, entry 4). It was found that the MW condition can raise the rate of the reaction without harmful to the environment and therefore reduced the energy consumption.

The HASIL was separated by simple filtration from the reaction mixture and it was washed with MeOH followed by acetone and dried in an oven at 100°C. Furthermore, the reusability of HASIL was screened. To investigate the catalytic efficiency of recycled HASIL, five successive cycles of the model reaction were run under optimal conditions. The activity of the catalyst did not show any significant decrease in the yields after five successive runs for the model reaction. It was found that the catalyst displayed good recyclability (Fig. 12).

The catalyst was further compared with previously reported catalysts (Table 5, entries 1–13), and the results are tabulated. In addition, Lewis acids such as $AlCl_3$, $ZnCl_2$, and CuBr were investigated for their catalytic activity; however, these Lewis acids proved to be ineffective for the reaction. The reaction with B $(OH)_3$ and $FeCl_3$ was also attempted, but the desired product was obtained in poor yield (Table 5, entries 14–18). The catalysts including montmorillonite K10, Fe $(HSO_4)_3$,

Table 6

Synthesis of quinolinyl and quinolonyl pyrans by using HASIL under MW conditions.

Entry	Aldehydes	1,3-Diketones	Product	Product	Time (min)	Yield (%)[a]
1	$C_{11}H_9NO_2$	$C_8H_{12}O_2$	$C_{22}H_{21}N_3O_3$	**4a**	10	97
2	$C_{17}H_{13}NO_2$	$C_8H_{12}O_2$	$C_{28}H_{25}N_3O_3$	**4b**	10	96
3	$C_{11}H_9NO_2$	$C_6H_{10}O_3$	$C_{20}H_{19}N_3O_4$	**4c**	10	96
4	$C_{11}H_9NO_2$	$C_3H_3NO_2S$	$C_{17}H_{12}N_4O_3S$	**4d**	12	90
5	$C_{11}H_8N_2O_4$	$C_3H_3NOS_2$	$C_{17}H_{11}N_5O_4S_2$	**4e**	15	88
6	$C_{11}H_8FNO_2$	$C_8H_{12}O_2$	$C_{22}H_{20}FN_3O_3$	**4f**	12	89
7	$C_{11}H_8FNO_2$	$C_6H_{10}O_3$	$C_{20}H_{18}FN_3O_4$	**4g**	14	92
8	$C_{11}H_8FNO_2$	$C_3H_3NO_2S$	$C_{17}H_{11}FN_4O_3S$	**4h**	15	87
9	$C_{10}H_6FNO_2$	$C_8H_{12}O_2$	$C_{21}H_{18}FN_3O_3$	**4i**	12	90
10	$C_{11}H_9NO_2$	$C_4H_4N_2O_3$	$C_{18}H_{13}N_5O_4$	**4j**	15	85
11	$C_{11}H_8ClNO$	$C_8H_{12}O_2$	$C_{22}H_{20}ClN_3O_2$	**4k**	12	89
12	$C_{12}H_{11}NO_2$	$C_8H_{12}O_2$	$C_{23}H_{23}N_3O_3$	**4l**	10	93
13	$C_{12}H_{11}NO_2$	$C_6H_{10}O_3$	$C_{21}H_{21}N_3O_4$	**4m**	10	95
14	$C_{12}H_{11}NO_2$	$C_3H_3NOS_2$	$C_{18}H_{14}N_4O_2S_2$	**4n**	10	93

[a]Isolated yields.

Scheme 4. Plausible mechanism for HASIL promoted synthesis of quinolinyl pyrans. HASIL, humic acid supported 1-butyl-3-methyl imidazolium thiocyanate. [Color figure can be viewed at wileyonlinelibrary.com]

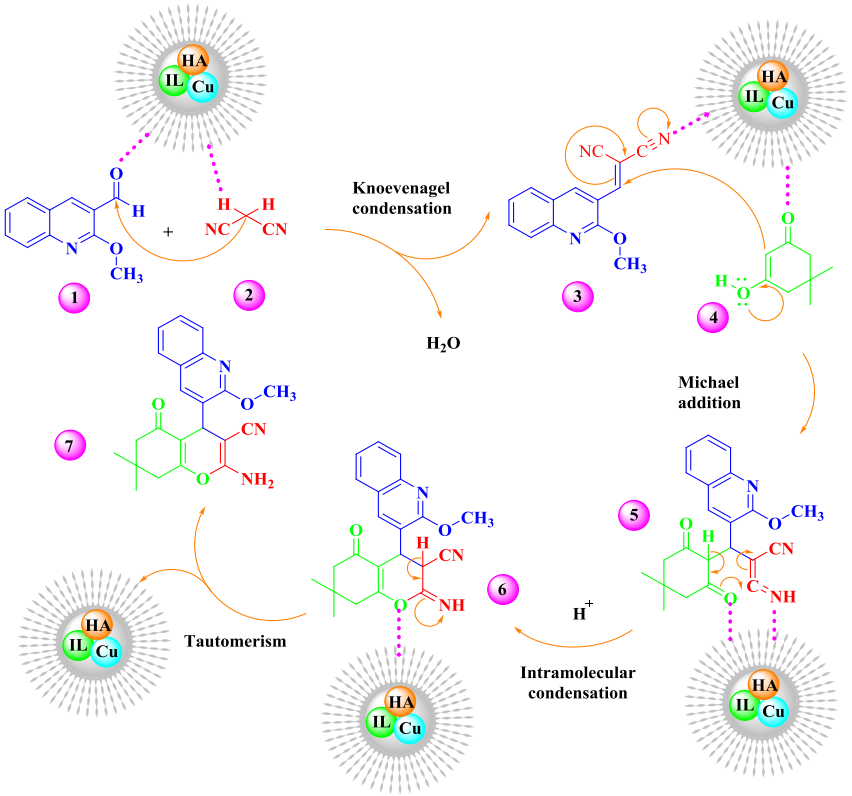

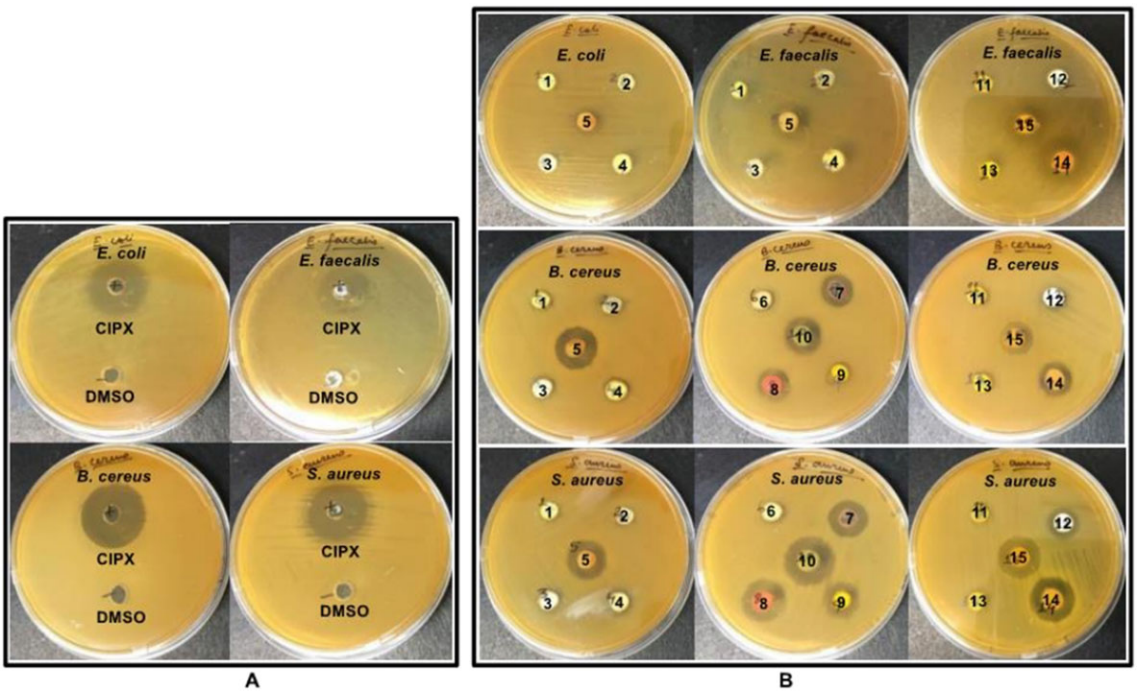

Figure 13. Growth inhibition of some bacterial strains caused by: (A) positive (ciprofloxacin) and negative (DMSO) control, (B) different derivatives of the quinolinyl pyrans. [Color figure can be viewed at wileyonlinelibrary.com]

Table 7
Antimicrobial screening test of the quinolinyl pyran derivatives against some bacterial strains.

Bacteria	Zone of inhibition by quinolinyl pyran derivatives														Ciprofloxacin (Positive control)
	1	2	3	4	5	6	7	8	9	10	11	12	13	14	15	
Bacillus cereus	0	0	0	0	19 ± 0.2	0	14 ± 0.4	14 ± 0.4	0	16 ± 0.3	0	0	0	13 ± 0.4	12 ± 0.3	25 ± 0.2
Staphylococcus aureus	0	0	0	0	16 ± 0.2	0	17 ± 0.3	16 ± 0.3	15 ± 0.2	21 ± 0.2	0	12 ± 0.4	0	19 ± 0.2	19 ± 0.2	24 ± 0.3
Escherichia coli	0	0	0	0	12 ± 0.3	0	0	0	0	0	0	0	0	0	0	25 ± 0.4
Enterococcus faecalis	0	0	0	0	14 ± 0.4	0	0	0	0	0	0	0	0	17 ± 0.3	13 ± 0.4	20 ± 0.6

1, **N/A**; 2, (**4i**); 3, (**4b**); 4, (**4k**); 5, (**4l**); 6, (**4c**); 7, (**4a**); 8, (**4d**); 9, (**4n**); 10, (**4h**); 11, (**4e**); 12, (**4j**); 13, (**4f**); 14, (**4m**); 15, (**4g**). Data are means of three replicates ($n = 3$) ± standard error.

TCT, $[DMAP\text{-}PEG_{1000}\text{-}DIL][BF_4]$, $[PhNMe_2CH_2NMe_2]Cl^-$, and DABCO offered more than 90% yield; however, they had drawbacks of long reaction times. It was deduced that the present protocol, with the aid of HASIL, was better than other reported protocols with respect to time, temperatures, and yields. Thus, the one-pot multicomponent synthesis of new quinolinyl pyrans was successfully synthesized by using HASIL under MW and characterized. A total of 14 compounds were synthesized successfully (Table 6). The FTIR, ^{1}H-NMR, and ^{13}C-NMR for all the synthesized compounds (**4a**–**4n)** are available in the Supporting Information.

Mechanism. Humic acid, a well-known cheap material, is able to catalyze the condensation of cyclic-1,3-diketones with aromatic aldehydes, and the products are formed with comparatively high yields [32]. The weak Van der Waals interaction and electrostatic interaction of [bmim]SCN IL [43] might be responsible for the catalytic activity.

A plausible mechanism is presented in Scheme 4. Herein, the active methylene group of malononitrile **2** attacks the carbonyl carbon of aldehyde **1** and undergoes Knoevenagel condensation to form **3** with loss of water. The methine carbon of the Knoevenagel product **3** is then activated by HASIL and it reacts with C—H activated compound **4** by a Michael addition to produce the intermediate **5**. Thereafter, **5** undergoes intramolecular cyclization to afford **6** followed by tautomerism, to produce the quinolinyl pyran **7**.

Antimicrobial studies. ***In vitro antibacterial properties of the quinolinyl and quinolonyl pyrans.*** The antibacterial efficacy was evaluated for quinolinyl-4*H*-pyrans (QPs) and quinolonyl-4*H*-pyrans (QOPs) by determining the zone of inhibition against a range of Gram-positive (*Bacillus cereus*, *Enterococcus faecalis*, and *Staphylococcus aureus*)

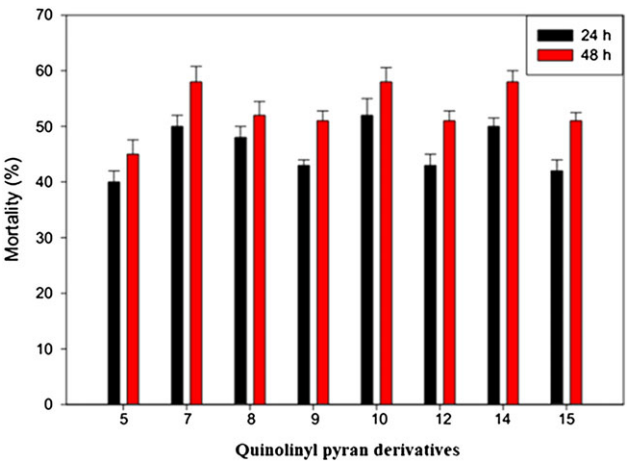

Figure 14. Quinolinyl pyrans (**4a**, **4d**, **4g**, **4h**, **4j**, **4l**, **4m**, and **4n**) toxicity assay at different intervals by *Artemia salina*. [Color figure can be viewed at wileyonlinelibrary.com]

Table 8

Molecular docking scores of quinolinyl pyran derivatives.

Entry	Molecule	Absolute energy	LibDock score
1	**4a**	43.92	96.69
2	**4b**	67.44	88.08
3	**4c**	59.67	74.59
4	**4d**	47.82	91.58
5	**4e**	58.46	85.14
6	**4f**	43.95	90.51
7	**4g**	66.08	96.30
8	**4h**	38.40	88.41
9	**4i**	61.69	78.97
10	**4j**	56.36	79.23
11	**4k**	41.66	92.11
12	**4l**	49.82	96.96
13	**4m**	67.50	82.32
14	**4n**	51.36	86.55
15	**Reference ligand**	83.08	176.61

and Gram-negative (*Escherichia coli*) bacteria (Fig. 13). It is found that **4a**, **4d**, **4h**, **4g**, and **4m** had preferential activity toward all Gram-positive species tested (Fig. 13). Moreover, compound **4j** and **4n** shows activity toward *S. aureus* only. Interestingly, compound **4l** shows their potential against all species tested (Table 7).

Quinolinyl-4*H*-pyrans that containing methoxy quinolines **4a**, **4m**, **and 4n**, sulfur heterocycles **4d** and **4h** and fluorinated quinolines **4g** and **4h** and QOP containing quinolonyl ring and methyl group **4j** showed remarkable potential effects toward Gram-positive bacteria. Interestingly, QP that contains methoxy and methyl group **4l** shows potential toward Gram-positive and Gram-negative bacteria. Fluorinated quinolinyl pyran **4g** and methyl QPs **4m** condensed from ethyl acetoacetate show potential toward Gram-negative. Thus, the core structure of quinoline and sulfur heterocyclic system from quinolinyl pyrans show crucial activity confirming the microbial effects of quinoline and sulfur heterocycles [3,15,19].

Antioxidant studies. ***2,2-Diphenyl-1-picrylhydrazyl scavenging activity of the quinolinyl-4H-pyrans and quinolonyl-4H-pyrans.*** The 2,2-diphenyl-1-picrylhydrazyl (DPPH) radical scavenging assay is used for initial screening of the compounds for their antioxidant activity [51]. An antioxidant assay was conducted for all QP derivatives and it was found that **4b**, **4d**, **4e**, **4f**, **4g**, **4h**, **4l**, **4m**, and **4n** are effective DPPH scavenging agents.

Toxicity assessment studies. ***Toxicity assessment of the quinolinyl-4H-pyrans and quinolonyl-4H-pyrans.*** Brine shrimp is one of the most valuable test organisms available for preliminary assessment of toxicity [52]. Therefore, the toxicity of all compounds at different intervals, which is having activity toward Gram-positive or Gram-negative or both species, was evaluated. Among all the compounds tested, **4d**, **4g**, **4l**, **4m**, and **4n** have mortality rate below 50% (Fig. 14), which suggest that these compounds are safe for further biological applications because less than 50% of brine shrimp mortality rate is considered as safe [53].

Molecular docking studies. The biological importance of quinolinyl pyran derivatives was assessed based on

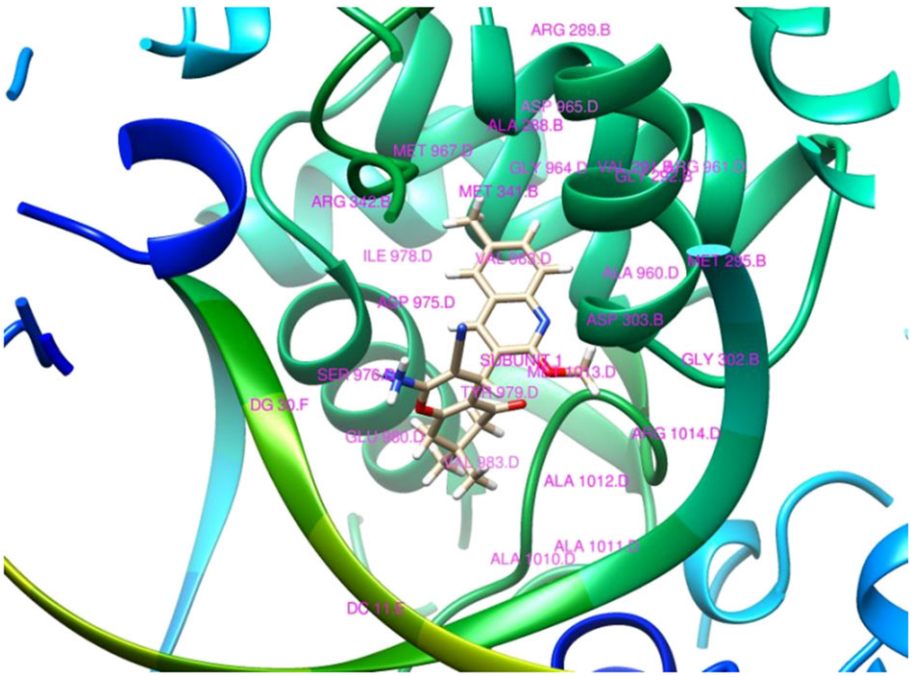

Figure 15. Ligand binding mode of **4l** inside Mtb DNA gyrase. [Color figure can be viewed at wileyonlinelibrary.com]

molecular docking. The crystal structure of Mtb gyrase (PDB ID: 4PLB) was used to determine the antibacterial activity of quinolinyl pyran derivatives [54]. The three dimensional structure of Mtb gyrase was prepared in Chimera software package to carry out molecular docking [55]. The ligands (QPs) were built in Chem3D Biodraw and were energetically minimized by MM2 method integrated with the same software. Further, ligands were prepared in for ionization, conformation, and stereoisomers in Discover Studio software packages [56]. Then, molecular docking was conducted using LibDock module of Discovery Studio software packages around the bound ligand. The docking pose of the ligands was ordered based on LibDock score (Table 8). The ligands were docked with the scores varying from 74.59 to 96.96 kcal/mol. The molecules **4a**, **4f**, **4g**, **4k**, and **4l** show higher binding affinity with the LibDock scores of 96.69, 92.11, 91.58, 90.51, 96.96, and 96.30, respectively, toward Mtb gyrase. Figure 15 shows the binding interaction of ligand **4l** inside Mtb DNA gyrase that strengthens the antimicrobial activity of **4l**.

CONCLUSION

In conclusion, a very simple, energy efficient, and conveniently practical method was developed for easy access to a wide range of pharmaceutically interesting functionalized quinolinyl and quinolonyl pyrans with catalytic amounts of HASIL. The reaction is a one-pot tandem Knoevenagel-cyclocondensation of aldehydes, malononitrile, and 1,3-diketones in ethanol at room temperature. Furthermore, seven QPs and one QOPs showed good potential against *B. cereus*, *E. faecalis*, *S. aureus*, and *E. coli* whilst nine QPs showed antioxidant properties. The brine shrimp test showed five QPs with mortality rate less than 50% until 48 h. Molecular docking showed one QP has remarkable interaction with Mtb DNA gyrase. Mild reaction conditions, excellent yields, operational simplicity, clean reaction profiles, energy efficiency, and high atom economy as well as the use of inexpensive and environmentally benign catalyst are the key advantages of the present method of synthesis. Moreover, the reusability of the catalyst is an added advantage to this protocol.

EXPERIMENTAL

Material and methods. All chemicals were purchased from Sigma-Aldrich and used without further purification. Solvents used were of synthesis grade. CEM discover MW reactor was used for reaction. The X-ray diffraction analysis was conducted with a Philips PW 1050 diffractometer set at 1 min with a scanning step size of 0.02 from 40 to 100 2 using monochromated CoK_{α} irradiation. Data were captured with a sietonics 122D automated microprocessor linked to diffractometer. A Carl Zeiss Ultra Plus scanning electron microscope with energy-dispersive X-ray spectroscopy detector was used. The TGA and DSC analyses were conducted with TA instruments. Melting points were determined by Stuart SMP10 and are uncorrected. The IR spectra were recorded on Perkin Elmer 537 spectrophotometer instrument, using ATR disc, and the absorption frequencies were expressed as ν_{max} cm^{-1}, ^{1}H-NMR and ^{13}C-NMR spectra were recorded on BRUKER 400 MHz spectrometer using tetramethylsilane as an internal standard. The chemical shift values are recorded on δ scale, and the coupling constants (J) are in hertz. The progress of the reaction was monitored by TLC using aluminum plates with silica gel (Sigma-Aldrich and Fluka). Silica gel (60–120 mesh) was purchased from Sigma-Aldrich and used as adsorbent for column chromatography. The elemental analyses (C, H, N) were obtained from a Perkin Elmer precisely 2400 analyzer.

General procedure for the synthesis of humic acid supported 1-butyl-3-methyl imidazolium thiocyanate catalyst. A mixture of [bmim]SCN (5 mmol) in methanol (10 mL) and HA (5 g) was taken in a round-bottomed flask (100 mL) and stirred at room temperature for 10 h under inert atmosphere and then dried under reduced pressure until free-flowing powder was obtained. In another round-bottomed flask (100 mL), [bmim]SCN (10 mmol) and copper acetate (0.5 mmol) were dissolved in methanol (10 mL) and stirred for 5 min. Thereafter, the HA pretreated with IL was suspended in this solution and the mixture was refluxed for 10 h under inert atmosphere. Then, solvent was evaporated under reduced pressure to get free-flowing powder. Then, it was dried in an oven at 200°C for 5 h to afford the HASIL catalyst.

Typical procedure for the synthesis of quinolinyl and quinolonyl pyrans. Catalytic amount (10 mol %) of HASIL was added to a mixture of aldehyde (1 mmol) and malononitrile (1 mmol) in ethanol (15 mL) followed by the addition of 1,3-diketone (1 mmol). The reaction tube was placed into a CEM MW discover synthesizer and irradiated at 120 W with the temperature of 110°C for 10 min. The progress of the reaction was monitored by TLC. After the completion of the reaction, the catalyst was separated by simple filtration. The solvent was evaporated under reduced pressure, and the crude product was purified by column chromatography using silica as adsorbent from eluent (ethyl acetate : petroleum ether, 50%). The crystallization of the product was performed in ethanol to yield the pure product.

Antibacterial activity of the quinolinyl and quinolonyl pyran derivatives. ***Bacterial strains.*** The antibacterial efficacy of each synthesized compound was assessed using four bacterial strains. Two strains of each Gram-positive (*B. cereus*, *S. aureus*, and *E. faecalis*) and Gram-negative (*E. coli*) bacteria were selected. The bacterial strains were provided from the culture collection of Department of Biotechnology and Food Technology, Durban University of Technology, South Africa.

Inoculum preparation. Each bacterial strain was subcultured overnight at 37°C on Mueller–Hilton agar plate. Further, bacterial cultures were grown in Mueller–Hilton broth at 37°C, 200 rpm in order to attain the viable count of approximately 10^8 cfu/mL.

Antibacterial activity. The agar well diffusion method was used to evaluate the antimicrobial activity of each compound. Hundred microliter of ~10^8 cfu/mL bacterial suspension was plated on Mueller–Hinton Agar plates. A well of 6 mm diameter was made using a sterile cork borer, and 30 μL of each compound (3 mg/mL) was added in each well and kept at 37°C for 16 h. The assays were carried out in triplicate. Ciprofloxacin (3 mg/mL) was used as positive control and DMSO (100%) as a negative control.

Antioxidant assays of the quinolinyl and quinolonyl pyran derivatives. The antioxidant ability of the quinolinyl pyran derivatives was determined by the decolorization of methanol solution of DPPH. Hundred microliter of each compound was added separately to 1 mL of 0.1-mM DPPH solution, and change in color was observed at regular intervals. Rutin hydrate was used as the positive control and methanol (95%) as negative control.

Toxicity assessment. The brine shrimp larvae (*Artemia salina*) were hatched in sea water for 24–48 h prior to being used in the test. An aliquot of 5 mL sea water containing 10 brine shrimp was added to each vial and supplemented with different derivatives of quinolinyl pyran. Each derivative concentrations of 300 μg was used in individual vial. Brine shrimp death was observed at regular intervals in order to find the toxic nature of each compound.

Synthesis of quinolinyl and quinolonyl pyrans (4a–4n) by using humic acid supported 1-butyl-3-methyl imidazolium thiocyanate under microwave conditions. ***2-Amino-4-(2-methoxyquinolin-3-yl)-7,7-dimethyl-5-oxo-5,6,7,8-tetrahydro-4H-chromene-3-carbonitrile (4a).*** Pale yellow crystals, mp = 182–184°C; IR ν_{max} (cm^{-1}): 2253 C≡N, 1571 C═N, 1216 C─N, 2970 CH, 1637 C═C, 1752 C═O, 2940 OCH_3, 3028 NH. ^{1}H-NMR: (400 MHz, $CDCl_3$) δ ppm 7.91 (1H, s, Ar─H), 7.79 (1H, d, J = 8.32 Hz, Ar─H), 7.65 (1H, d, J = 1.4 Hz, Ar─H), 7.58 (1H, td, J = 1.24 Hz, Ar─H), 7.38 (1H, td, J = 8.28 Hz, Ar─H), 4.68 (1H, s, CH), 4.59 (2H, brs, NH_2), 4.08 (3H, brs, OCH_3), 2.48 (2H, q, J = 1.04 Hz, CH_2), 2.22 (2H, q, J = 18 Hz, CH_2), 1.14 (3H, brs, CH_3), 1.05 (3H, brs, CH_3). ^{13}C-NMR: (100 MHz, $CDCl_3$) δ ppm 195.9, 162.9, 160.1, 158.6, 137.8, 129.2, 127.6, 126.6, 126.6, 125.3, 125.2, 124.0, 111.8, 60.8, 53.4, 50.5, 40.7, 32.7, 32.1, 29.3, 27.0. Elemental Analysis: *Anal*. Calcd for $C_{22}H_{21}N_3O_3$: C, 70.38; H, 5.64; N, 11.19; %. Found: C, 70.36; H, 5.65; N, 11.20; %.

2-Amino-7,7-dimethyl-5-oxo-4-(2-(o-tolyloxy)quinolin-3-yl)-5,6,7,8-tetrahydro-4H-chromene-3-carbonitrile (4b). Yellow solid, mp = 209–211°C; IR ν_{max} (cm^{-1}): IR ν_{max} (cm^{-1}): 2246 C≡N, 1577 C═N, 1207 C─N, 2924 CH, 1631 C═C, 1751 C═O, 3327 NH. ^{1}H-NMR: (400 MHz, DMSO-d_6) δ ppm 8.69 (1H, s, Ar─H), 8.05 (2H, d, J = 7.84 Hz, Ar─H), 7.92 (2H, d, J = 8.32 Hz, Ar─H), 7.84 (2H, td, J = 1.36 Hz, Ar─H), 7.63 (2H, td, J = 1.04 Hz, Ar─H), 5.21 (1H, s, CH), 4.98 (2H, s, NH_2), 3.01 (3H, brs, CH_3), 2.70 (2H, q, J = 17.88 Hz, CH_2), 2.41 (2H, q, J = 16.16 Hz, CH_2), 1.14 (3H, brs, CH_3), 1.12 (3H, brs, CH_3). ^{13}C-NMR: (100 MHz, DMSO-d_6) δ ppm 195.6, 169.0, 154.5, 145.5, 140.6, 131.5, 128.0, 127.5, 126.6, 126.6, 113.8, 112.8, 112.6, 107.2, 49.6, 40.4, 40.0, 39.8, 39.6, 39.4, 39.2, 38.8, 33.2, 31.7, 30.5, 28.9, 27.1, 26.0. Elemental Analysis: *Anal*. Calcd for $C_{28}H_{25}N_3O_3$: C, 74.48; H, 5.58; N, 9.31; %. Found: C, 74.47; H, 5.59; N, 9.33; %.

Methyl 6-amino-5-cyano-4-(2-methoxyquinolin-3-yl)-2-methyl-4H-pyran-3-carboxylate (4c). Yellow solid, mp = 209–211°C; IR ν_{max} (cm^{-1}): 2254 C≡N, 1552 C═N, 1226 C─N, 2970 CH, 1672 C═C, 1722 C═O, 2876 OCH_3, 3361 NH. ^{1}H-NMR: (400 MHz, DMSO-d_6) δ ppm 8.92 (1H, s, Ar─H), 8.21 (1H, d, J = 6.40 Hz, Ar─H), 7.78 (1H, dd, J = 2.52 Hz, Ar─H), 7.52 (1H, dt, J = 1.12 Hz, Ar─H), 7.30 (1H, t, J = 5.56 Hz, Ar─H), 6.98 (2H, brs, NH_2), 4.59 (1H, s, CH), 3.76 (3H, s, OCH_3), 2.59 (2H, q, J = 13.52 Hz, CH_2), 1.95 (3H, s, CH_3), 1.23 (3H, s, CH_3). ^{13}C-NMR: (100 MHz, DMSO-d_6) δ ppm 165.4, 158.4, 156.5, 144.8, 128.3, 127.1, 126.7, 119.6, 107.2, 60.1, 57.2, 40.0, 39.8, 39.6, 39.0, 38.8, 38.7, 30.6, 18.0, 13.6. Elemental Analysis: *Anal*. Calcd for $C_{20}H_{19}N_3O_4$: C, 65.74; H, 5.24; N, 11.50; %. Found: C, 65.76; H, 5.26; N, 11.51; %.

5-Amino-7-(2-methoxyquinolin-3-yl)-2-oxo-3,7-dihydro-2H-pyrano[2,3-d]thiazole-6-carbonitrile (4d). Yellow solid, mp = 218–220°C; IR ν_{max} (cm^{-1}): 2191 C≡N, 1604 C═N, 1215 C─N, 2970 CH, 1654 C═C, 1751 C═O, 2863 OCH_3, 714 C─S, 2596 S─H, 3393 NH. ^{1}H-NMR: (400 MHz, DMSO-d_6) δ ppm 10.25 (2H, s, NH_2), 8.41 (1H, s, Ar─H), 7.79 (1H, d, J = 7.44 Hz, Ar─H), 7.56 (1H, t, J = 7.12 Hz, Ar─H), 7.34 (1H, d, J = 8.28 Hz, Ar─H), 7.17 (1H, t, J = 7.24 Hz, Ar─H), 5.13 (1H, s, NH), 4.42 (1H, s, CH), 2.51 (3H, s, OCH_3). ^{13}C-NMR: (100 MHz, $CDCl_3$) δ ppm 159.8, 159.8, 153.1, 150.7, 145.8, 136.8, 136.7, 134.4, 134.2, 134.1, 129.7, 127.7, 126.7, 125.1, 125.1, 124.5, 124.5, 124.3, 120.8, 120.8, 118.2, 118.1, 114.8, 114.6, 113.1, 113.1, 63.6, 63.5, 63.3, 63.2, 54.0, 49.3, 47.8, 16.4, 16.4, 16.2, 16.1.

Elemental Analysis: *Anal*. Calcd for $C_{17}H_{12}N_4O_3S$: C, 57.95; H, 3.43; N, 15.90; %. Found: C, 57.97; H, 3.44; N, 15.92; %.

5-Amino-7-(2-methoxy-6-nitroquinolin-3-yl)-2-thioxo-3,7-dihydro-2H-pyrano[2,3-d]thiazole-6-carbonitrile (4e). Brown solid, mp = 249–251°C; IR ν_{max} (cm^{-1}): 2254 C≡N, 1588 C═N, 1047 C─N, 2880 CH, 1608 C═C, 1709 C═O, 2944 OCH_3, 2602 S─H, 1268 C═S, 650 C─S, 3232 NH. ^{1}H-NMR: (400 MHz, DMSO-d_6) δ ppm 8.15 (1H, s, NH), 7.78 (1H, s, Ar─H), 7.65 (2H, d, J = 10.24 Hz, Ar─H), 7.55 (1H, d, J = 8.44 Hz, Ar─H), 6.80 (2H, brs, NH_2), 4.25 (1H, s, CH), 4.03 (3H, s, OCH_3). ^{13}C-NMR: (100 MHz, $CDCl_3$) δ ppm 150.2, 150.1, 147.0, 146.9, 145.3, 145.1, 139.3, 137.8, 137.7, 130.7, 129.2, 129.1, 129.1, 128.0, 127.9, 127.3, 127.2, 119.9, 114.4, 110.6, 63.9, 63.9, 63.5, 63.4, 52.5, 51.0, 21.5, 16.4, 16.4, 16.1, 16.1, 16.0. Elemental Analysis: *Anal*. Calcd for $C_{17}H_{11}N_5O_4S_2$: C, 49.39; H, 2.68; N, 16.94; %. Found: C, 49.41; H, 2.70; N, 16.96; %.

2-Amino-4-(7-fluoro-2-methoxyquinolin-3-yl)-7,7-dimethyl-5-oxo-5,6,7,8-tetrahydro-4H-chromene-3-carbonitrile (4f). White solid, mp = 195–197°C; IR ν_{max} (cm^{-1}): 2181 C≡N, 1602 C═N, 1135 C─N, 2970 CH, 1638 C═C, 1678 C═O, 2653 OCH_3, 1007 C─F, 3368 NH. ^{1}H-NMR: (400 MHz, DMSO-d_6) δ ppm 8.03 (1H, s, Ar─H), 7.96 (1H, t, J = 6.44 Hz, Ar─H), 7.46 (1H, d, J = 2.52 Hz, Ar─H), 7.33 (1H, t, J = 6.20 Hz, Ar─H), 7.01 (2H, brs, NH_2), 4.52 (1H, s, CH), 3.96 (3H, s, OCH_3), 2.49 (2H, q, J = 17.80 Hz, CH_2), 2.24 (2H, q, J = 16.04 Hz, CH_2), 1.04 (3H, s, CH_3), 0.96 (3H, s, CH_3). ^{13}C-NMR: (100 MHz, $CDCl_3$) δ ppm 155.6, 148.5, 146.4, 146.3, 137.3, 129.2, 129.0, 123.0, 123.0, 122.9, 122.9, 119.7, 118.5, 114.0, 63.6, 63.5, 63.3, 63.2, 58.3, 56.8, 16.4, 16.3, 16.2, 16.1. ^{19}F-NMR: (400 MHz, $CDCl_3$) −107.33. Elemental Analysis: *Anal*. Calcd for $C_{22}H_{20}FN_3O_3$: C, 67.17; H, 5.12; N, 10.68; %. Found: C, 67.19; H, 5.14; N, 10.70; %.

Ethyl-6-amino-5-cyano-4-(7-fluoro-2-methoxyquinolin-3-yl)-2-methyl-4H-pyran-3-carboxylate (4g). Yellow solid, mp = 191–193°C; IR ν_{max} (cm^{-1}): 2229 C≡N, 1580 C═N, 1219 C─N, 2919 CH, 1614 C═C, 1708 C═O, 1021 C─F, 3400 NH. ^{1}H-NMR: (400 MHz, DMSO-d_6) δ ppm 8.87 (1H, s, Ar─H), 8.59 (1H, s, Ar─H), 8.02 (1H, d, J = 8.04 Hz, Ar─H), 7.83 (2H, s, NH_2), 7.54 (1H, t, J = 2.88 Hz, Ar─H), 4.43 (1H, s, CH), 4.07 (3H, s, OCH_3), 3.91–3.89 (2H, m, J = 16.88 Hz, CH_2), 2.50 (3H, s, CH_3), 2.39 (3H, s, CH_3). ^{13}C-NMR: (100 MHz, $CDCl_3$) δ ppm 176.0, 176.0, 156.2, 155.4, 155.3, 151.5, 151.4, 139.2, 134.2, 126.2, 125.9, 125.8, 123.2, 119.5, 118.3, 112.3, 64.0, 63.9, 63.9, 63.8, 45.6, 44.0, 29.6, 16.4, 16.4, 16.3, 16.2, 14.1. Elemental Analysis: *Anal*. Calcd for $C_{20}H_{18}FN_3O_4$: C, 62.66; H, 4.73; N, 10.96; %. Found: C, 62.68; H, 4.75; N, 10.95; %.

5-Amino-7-(7-fluoro-2-methoxyquinolin-3-yl)-2-oxo-3,7-dihydro-2H-pyrano[2,3-d]thiazole-6-carbonitrile (4h). Brown solid, mp = 205–207°C; IR ν_{max} (cm^{-1}): 2252 C≡N, 1557 C═N, 1292 C─N, 2917 CH, 1621 C═C, 1690 C═O, 2849 OCH_3, 693 C─S, 2606 S─H, 1393 C─F, 3362 NH. ^{1}H-NMR: (400 MHz, $CDCl_3$) δ ppm 8.42 (1H, s, NH), 8.35 (1H, d, J = 3.12 Hz, Ar─H), 8.17 (2H, s, NH_2), 7.80 (1H, d, J = 5.68 Hz, Ar─H), 7.68 (1H, t, J = 7.08 Hz, Ar─H), 7.42 (1H, t, J = 7.24 Hz, Ar─H), 4.91 (1H, s, CH), 2.25 (3H, s, OCH_3).^{13}C-NMR: (100 MHz, $CDCl_3$) δ ppm 206.9, 163.5, 147.9, 147.8, 145.9, 142.3, 137.9, 129.1, 122.8, 121.3, 113.8, 32.9, 32.9, 32.7, 30.9, 22.2, 13.7. Elemental Analysis: *Anal*. Calcd for $C_{17}H_{11}FN_4O_3S$: C, 55.13; H, 2.99; N, 15.13; %. Found: C, 55.15; H, 2.98; N, 15.15; %.

2-Amino-4-(7-fluoro-2-oxo-1,2-dihydroquinolin-3-yl)-7,7-dimethyl-5-oxo-5,6,7,8-tetrahydro-4H-chromene-3-carbonitrile (4i). Pale yellow, mp = 129–131°C; IR ν_{max} (cm^{-1}): 2183 C≡N, 1572 C═N, 1152 C─N, 2979 CH, 1679 C═C, 1722 C═O, 1098 C─F, 3446 NH. ^{1}H-NMR: (400 MHz, DMSO-d_6) δ ppm 8.69 (1H, s, NH), 8.40 (1H, s, Ar─H), 8.10–8.04 (1H, m, J = 6.24 Hz, Ar─H), 7.73 (2H, s, NH_2), 7.50 (1H, t, J = 5.84 Hz, Ar─H), 7.42 (1H, s, Ar─H), 4.09 (1H, s, CH), 2.70–2.57 (2H, m, J = 17.92 Hz, CH_2), 2.40–2.28 (2H, m, J = 16.20 Hz, CH_2), 1.25 (3H, s, CH_3), 1.05 (3H, s, CH_3). ^{19}F-NMR: (400 MHz, DMSO-d_6) δ ppm −108.37. ^{13}C-NMR: (100 MHz, $CDCl_3$) δ ppm 195.6, 191.2, 161.9, 140.5, 138.1, 130.1, 126.3, 126.1, 123.9, 122.4, 121.0, 120.5, 119.0, 117.6, 109.3, 108.7, 108.5, 96.6, 37.7, 29.0, 24.8, 19.8, 13.8, 13.7. Elemental Analysis: *Anal*. Calcd for $C_{21}H_{18}FN_3O_3$: C, 66.48; H, 4.78; N, 11.08; %. Found: C, 66.50; H, 4.79; N, 11.10; %.

7-Amino-5-(6-methyl-2-oxo-1,2-dihydroquinolin-3-yl)-2,4-dioxo-1,3,4,5-tetrahydro-2H-pyrano[2,3-d]pyrimidine-6-carbonitrile (4j). Brown solid, mp = 237–239°C; IR ν_{max} (cm^{-1}): 2222 C≡N, 1572 C═N, 1217 C─N, 2925 CH, 1651 C═C, 1750 C═O, 3026 NH. ^{1}H-NMR: (400 MHz, DMSO-d_6) δ ppm 12.20 (1H, s, NH), 10.78 (1H, s, NH), 9.42 (1H, s, NH), 8.12 (1H, s, Ar─H), 7.55 (1H, d, J = 1.44 Hz, Ar─H), 7.46 (2H, t, J = 8.44 Hz, Ar─H), 7.29 (2H, s, NH_2), 4.44 (1H, s, CH), 2.36 (3H, brs, CH_3). ^{13}C-NMR: (100 MHz, $CDCl_3$) δ ppm 159.8, 159.8, 145.9, 145.9, 144.5, 144.3, 136.7, 136.6, 129.7, 129.1, 127.7, 126.8, 125.1, 125.1, 124.3, 123.2, 120.6, 120.6, 114.7, 63.6, 63.5, 63.4, 63.3, 53.9, 49.6, 48.1, 16.4, 16.4, 16.1, 16.1. Elemental Analysis: *Anal*. Calcd for $C_{18}H_{13}N_5O_4$: C, 59.50; H, 3.61; N, 19.28; %. Found: C, 59.52; H, 3.63; N, 19.30; %.

2-Amino-4-(2-chloro-6-methylquinolin-3-yl)-7,7-dimethyl-5-oxo-5,6,7,8-tetrahydro-4H-chromene-3-carbonitrile (4k). Yellow solid, mp = 187–189°C; IR ν_{max} (cm^{-1}): 2227 C≡N, 1562 C═N, 1216 C─N, 2923 CH, 1657 C═C, 1751 C═O, 733 C─Cl, 3039 NH. ^{1}H-NMR: (400 MHz, DMSO-d_6) δ ppm 11.38 (2H, s, NH_2), 7.71 (1H, d, J = 3.2 Hz, Ar─H), 7.47 (1H, s, Ar─H), 7.35–7.32 (1H, t, J = 2.52 Hz, Ar─H), 7.30–7.27 (1H, d, J = 5.56 Hz,

Ar—H), 4.51 (1H, s, CH), 2.52 (3H, brs, CH_3), 2.39 (2H, q, J = 16.25 Hz, CH_2), 2.25 (2H, q, J = 12.36 Hz, CH_2), 1.32 (3H, s, CH_3), 0.92 (3H, s, CH_3). ^{13}C-NMR: (100 MHz, $CDCl_3$) δ ppm 176.2, 176.2, 156.2, 155.3, 155.2, 145.2, 145.0, 133.8, 129.3, 125.9, 125.4, 123.4, 120.0, 119.1, 118.2, 114.0, 63.8, 63.7, 63.5, 63.4, 46.2, 44.6, 30.9, 16.4, 16.3, 16.2, 16.2. Elemental Analysis: *Anal*. Calcd for $C_{22}H_{20}ClN_3O_2$: C, 67.09; H, 5.12; N, 10.67; %. Found: C, 67.10; H, 5.14; N, 10.69; %.

2-Amino-4-(2-methoxy-6-methylquinolin-3-yl)-7,7-dimethyl-5-oxo-5,6,7,8-tetrahydro-4H-chromene-3-carbonitrile (4l). Yellow solid, mp = 174–176°C; IR ν_{max} (cm^{-1}): 2223 C≡N, 1579 C═N, 1236 C—N, 2840 CH, 1614 C═C, 1697 C═O, 2970 OCH_3, 3446 NH. ^{1}H-NMR: (400 MHz, $CDCl_3$) δ ppm 7.72 (1H, s, Ar—H), 7.60 (1H, d, J = 8.48 Hz, Ar—H), 7.39 (1H, s, Ar—H), 7.32 (1H, dd, J = 1.60 Hz, Ar—H), 4.68 (2H, brs, NH_2), 4.54 (1H, s, CH), 3.98 (3H, s, OCH_3), 2.37 (3H, s, CH_3), 2.34 (2H, q, J = 12.20 Hz, CH_2), 2.17 (2H, q, J = 16.44 Hz, CH_2), 1.02 (3H, s, CH_3), 0.93 (3H, s, CH_3). ^{13}C-NMR: (100 MHz, $CDCl_3$) δ ppm 196.0, 162.9, 159.7, 158.7, 144.0, 137.2, 133.5, 131.2, 126.7, 126.3, 125.3, 125.3, 119.0, 111.8, 60.4, 53.3, 50.5, 40.7, 32.6, 32.1, 29.2, 27.0, 21.2. Elemental Analysis: *Anal*. Calcd for $C_{23}H_{23}N_3O_3$: C, 70.93; H, 5.95; N, 10.79; %. Found: C, 70.95; H, 5.96; N, 10.81; %.

Ethyl-6-amino-5-cyano-4-(2-methoxy-6-methylquinolin-3-yl)-2-methyl-4H-pyran-3-carboxylate (4m). Brown solid, mp = 188–190°C; IR ν_{max} (cm^{-1}): 2338 C≡N, 1512 C═N, 1240 C—N, 2917 CH, 1627 C═C, 1697 C═O, 2879 OCH_3, 3233 NH. ^{1}H-NMR: (400 MHz, DMSO-d_6) δ ppm 8.30 (1H, s, Ar—H), 7.46 (1H, d, J = 3.12 Hz, Ar—H), 7.11 (2H, dt, J = 10.20 Hz, Ar—H), 7.05 (2H, brs, NH_2), 4.17 (1H, s, CH), 2.49 (3H, s, OCH_3), 2.06 (2H, q, J = 16.04 Hz, CH_2), 1.48 (3H, s, CH_3), 1.02 (3H, s, CH_3), 0.94 (3H, s, CH_3). ^{13}C-NMR: (100 MHz, $CDCl_3$) δ ppm 165.0, 163.0, 160.3, 150.6, 145.7, 142.9, 136.0, 135.3, 130.5, 130.4, 129.9, 129.1, 128.1, 127.4, 126.8, 125.4, 124.0, 120.5, 103.4, 62.0, 61.0, 60.8, 53.5, 33.6, 13.8, 13.4. Elemental Analysis: *Anal*. Calcd for $C_{21}H_{21}N_3O_4$: C, 66.48; H, 5.58; N, 11.08; %. Found: C, 66.50; H, 5.59; N, 11.10; %.

5-Amino-7-(2-methoxy-6-methylquinolin-3-yl)-2-thioxo-3,7-dihydro-2H-pyrano[2,3-d]thiazole-6-carbonitrile (4n). Brown solid, mp = 198–200°C; IR ν_{max} (cm^{-1}): 2226 C≡N, 1557 C═N, 1229 C—N, 2927 CH, 1688 C═C, 1751 C═O, 2826 OCH_3, 1074 C═S, 615 C—S, 2511 S—H, 3407 NH. ^{1}H-NMR: (400 MHz, DMSO-d_6) δ ppm 12.07 (1H, brs, NH), 8.49 (1H, s, Ar—H), 7.82 (1H, d, J = 5.88 Hz, Ar—H), 7.74 (2H, dd, J = 3.96 Hz, Ar—H), 7.46 (2H, brs, NH_2), 4.69 (1H, s, CH), 3.63 (3H, s, OCH_3), 2.39 (3H, s, CH_3). ^{13}C-NMR: (100 MHz, $CDCl_3$) δ ppm 190.4, 189.3, 135.2, 134.9, 128.9, 126.6, 115.7, 77.4, 47.0, 46.4, 40.9, 32.4, 31.4, 29.6, 29.2, 27.4, 20.9. Elemental Analysis: *Anal*. Calcd for $C_{18}H_{14}N_4O_2S_2$: C, 56.53; H, 3.69; N, 14.65; %. Found: C, 56.55; H, 3.71; N, 14.67; %.

Acknowledgments. We are grateful to the National Research Foundation (NRF) and Durban University of Technology (DUT) (grant number MT21356991) for funding this project.

REFERENCES AND NOTES

[1] Abe, I.; Oguro, S.; Utsumi, Y.; Sano, Y.; Noguchi, H. J Am Chem Soc 2005, 127, 12709.

[2] Sibi, M. P.; Zimmerman, J. J Am Chem Soc 2006, 128, 13346.

[3] Hussein, A. H. M.; Gad-Elkareem, M. A.; El-Adasy, A. B. A.; Khames, A. A.; Othman, I. M. Int J Org Chem 2012, 2, 341.

[4] Chattapadhyay, T. K.; Dureja, P. J. Agri and Food Chem 2006, 54, 2129.

[5] Wang, T.; Liu, J.; Zhong, H.; Chen, H.; Lv, Z.; Zhang, Y.; Zhang, M.; Geng, D.; Niu, C.; Li, Y.; Li, K. Bioorg Med Chem Lett 2011, 21, 3381.

[6] DeSimone, R. W.; Currie, K. S.; Mitchell, S. A.; Darrow, J. W.; Pippin, D. A. Chem & High Throughput Screen 2004, 7, 473.

[7] Safari, J.; Zarnegar, Z.; Heydarian, M. Bull Chem Soc Japan 2012, 85, 1332.

[8] Bonsignore, L.; Loy, G.; Secci, D.; Calignano, A. Eur J Med Chem 1993, 28, 517.

[9] Heravi, M. M.; Baghernejad, B.; Oskooie, H. A. J Chin Chem Soc 2008, 55, 659.

[10] Hatakeyama, S.; Ochi, N.; Numata, H.; Takano, S. J. Chem Soc, Chem Comm 1988, 17, 1202.

[11] Singh, K.; Singh, J.; Singh, H. Tetrahedron 1996, 52, 14273.

[12] Armesto, D.; Horspool, W. M.; Martin, N.; Ramosand, A.; Seoane, C. J Organomet Chem 1989, 54, 3069.

[13] Maleki, B.; Sheikh, S. Org Preparation and Pro Int 1989, 47, 368.

[14] Kumar, D.; Reddy, V. B.; Sharad, S.; Dube, U.; Kapur, S. Eur J Med Chem 2009, 44, 3805.

[15] (a) Elderfield, R. C. Heterocyclic Compounds; John Wiley: New York, London, 1960; (b) Wright, C. W.; Addae-Kyereme, J.; Breen, A. G.; Brown, J. E.; Cox, M. F.; Croft, S. L.; Gökçek, Y.; Kendrick, H.; Phillips, R. M.; Pollet, P. L. J Med Chem 2001, 44, 3187; (c) Sahu, N. P.; Pal, C.; Mandal, N. B.; Banerjee, S.; Raha, M.; Kundu, A. P.; Basu, A.; Ghosh, M.; Roy, K.; Bandyopadhyay, S. Bioorg Med Chem 2002, 10, 1687; (d) Bringmann, G.; Reichert, Y.; Kane, V. V. Tetrahedron 2004, 60, 3539; (e) Kouznetsov, V. V.; Méndezand, L. Y. V.; Gómez, C. M. M. Curr Org Chem 2005, 9, 141.

[16] Peters, W.; Richards, W. H. G. Antimalarial Drug II; Springer Verlag: Berlin Heidelberg, New York, Tokyo, 1984.

[17] (a) Corral, R. A.; Orazi, O. O. Tetrahedron Lett 1967, 8, 583; (b) Sekar, M.; Prasad, K. R. J Nat Prod 1998, 61, 294; (c) Puricelli, L.; Innocenti, G.; Monache, G. D.; Caniato, R.; Filippini, R.; Cappelletti, E. M. Nat Prod Lett 2002, 16, 95; (d) Marco, J. L. Mini-Rev Med Chem 2003, 3, 518; (e) Pandit, K. S.; Chavan, P. V.; Desai, U. V.; Kulkarni, M. A.; Wadgaonkar, P. P. New J Chem 2015, 39, 4452.

[18] Morel, A. F.; Larghi, E. L. Tetrahedron Asymmetry 2004, 15, 9.

[19] (a) Metzner, P.; Thuillier, A. Sulfur Reagents in Organic Synthesis; Academic Press: New York, 1994; (b) Nudelman, A. The Chemistry of Optically Active Sulfur Compounds; Gordon and Breach: New York, 1984; (c) Chatgilialoglu, C.K.; Asmus, D. Springer: New York, 1991.

[20] Bicking, J. B.; Holtz, W. J.; Watson, L. S.; Cragoe, E. J. Jr. J Med Chem 1976, 19, 530.

[21] Ghosh, A. K.; Thompson, W. J.; McKee, S. P.; Duong, T. T.; Lyle, T. A.; Chen, J. C.; Darke, P. L.; Zugay, J. A.; Emini, E. A. J Med Chem 1993, 36, 292.

[22] Inomata, K.; Barragué, M.; Paquette, L. A. The J Org Chem 2005, 70, 533.
[23] Yamauchi, M.; Katayama, S.; Watanabe, T. Synthesis 1982, 11, 935.
[24] Evdokimov, N. M.; Kireev, A. S.; Yakovenko, A. A.; Antipin, M. Y.; Magedov, I. V.; Kornienko, A. J Organomet Chem 2007, 72, 3443.
[25] Wasserscheid, P.; Welton, T. Ionic Liquids in Synthesis; Wiley-VCH: Weinheim, 2008.
[26] Weingärtner, H. Angew Chem Int Ed 2008, 47, 654.
[27] Wasserchеid, P.; Keim, W. Angew Chem Int Ed 2000, 39, 3772.
[28] Mehnert, C. P. Chem Eur J 2005, 11, 50.
[29] Riisagera, A.; Fehrmanna, R.; Haumannb, M.; Wasserscheidb, P. Top Catal 2006, 40, 91.
[30] Gu, Y.; Li, G. Adv Synth Catal 2009, 351, 817.
[31] Van Doorslaer, C.; Wahlen, J.; Mertens, P.; Binnemans, K.; De Vos, D. Dalton Trans 2010, 39, 8377.
[32] Kļaviņš, M.; Dipāne, J.; Babre, K. Chemosphere 2001, 44, 737.
[33] Lü, R.; Qu, Z.; Lin, J. J Mol Liq 2013, 180, 207.
[34] Wilmer, H.; Genger, T.; Hinrichsen, O. J Catal 2003, 215, 188.
[35] Chilom, G.; Rice, J. A. Org Geochem 2005, 36, 1339.
[36] Visser, S. A.; Mendel, H. Soil Biol Biochem 1971, 3, 259IN17263.
[37] Das, G.; Kalita, R. D.; Gogoi, P.; Buragohain, A. K.; Karak, N. Appl Clay Sci 2014, 90, 18.
[38] Xu, D.; Zhu, S.; Chen, H.; Li, F. Colloids Surf A Physicochem Eng Asp 2006, 276, 1.
[39] Pandey, A. K.; Pandey, S. D.; Misra, V. Ecotoxicol Environ Saf 2000, 47, 195.
[40] Changlung, C.; Wang, X.; Jiang, H.; Hu, E. Colloids Surf A Physicochem Eng Asp 2007, 302, 121.
[41] Zhang, J.; Dai, J.; Wang, R.; Li, F.; Wang, W. Colloids Surf A Physicochem Eng Asp 2009, 335, 194.
[42] Sîrbu, C. E.; Cioroianu, T. M.; Rotaru, P. Physics AUC 2010, 20, 120.
[43] Dharaskar, S. A.; Wasewar, K. L.; Varma, M. N.; Shende, D. Z. Environ Sci Pollut Res 2016, 23, 9284.
[44] Kučerík, J.; Kovář, J.; Pekař, M.; Šimon, P. Naturwissenschaften 2005, 92, 336.
[45] Gibbs, H. A.; O'Garro, L. W.; Newton, A. M. Thermochim Acta 2001, 374, 137.
[46] Válková, D.; Kislinger, J.; Pekař, M.; Kučerík, J. J Ther Analysis and Calor 2007, 89, 957.
[47] Dell'Abate, M. T.; Benedetti, A.; Trinchera, A.; Dazzi, C. Geoderma 2002, 107, 281.
[48] Fernandez, J. M.; Plante, A. F.; Leifeld, J.; Rasmussen, C. J Therm Anal Calorim 2011, 104, 389.
[49] Mohabey, S.; Mohabey, H. Mat Sci Research India 2014, 11, 63.
[50] Nayak, G.; Shrivastava1, B.; Singhai, A. K. Orient J Chem 2016, 32, 1977.
[51] Sowndhararajan, K.; Kang, S. C. Saudi J Bio Sci 2013, 20, 319.
[52] Rajabi, S.; Ramazani, A.; Hamidiand, M.; Naji, T. DARU J Phar Sciences 2015, 23, 20.
[53] Meyer, B. N.; Ferrigni, N. R.; Putnam, J. E.; Jacobsen, L. B.; Nichols, D. J.; McLaughlin, J. L. Planta Med 1982, 45, 31.
[54] Singh, S. B.; Kaelin, D. E.; Wu, J.; Miesel, L.; Tan, C. M.; Meinke, P. T.; Olsen, D.; Lagrutta, A.; Bradley, P.; Lu, J.; Patel, S. ACS Med Chem Lett 2014, 5, 609.
[55] Pettersen, E. F.; Goddard, T. D.; Huang, C. C.; Couch, G. S.; Greenblatt, D. M.; Meng, E. C.; Ferrin, T. E. J Comput Chem 2004, 25, 1605.
[56] Biovia, D.S. San Diego: Dassault Systemes, 2015.
[57] Kantevari, S.; Vuppalapati, S. V.; Nagarapu, L. Catal Commun 2007, 8, 1857.
[58] Shaterian, H. R.; Yarahmadi, H.; Ghashang, M. Bioorg Med Chem Lett 2008, 18, 788.
[59] Kundu, D.; Majee, A.; Hajra, A. Catal Commun 2010, 11, 1157.
[60] Das, B.; Laxminarayana, K.; Ravikanth, B.; Rao, B. R. J Mol Catalysis A: Chemical 2007, 261, 180.
[61] Zhang, P.; Zhang, Z. H. Monatshefte für Chemie-Chemical Monthly 2009, 140, 199.
[62] Khodaei, M. M.; Khosropour, A. R.; Moghanian, H. Synlett 2006, 6, 916.
[63] Nagarapu, L.; Baseeruddin, M.; Apuri, S.; Kantevari, S. Catal Commun 2007, 8, 1729.
[64] Rashinkar, G.; Salunkhe, R. J Mol Catalysis A: Chemical 2010, 316, 146.
[65] Hajipour, A. R.; Ghayeb, Y.; Sheikhan, N.; Ruoho, A. E. Tetrahedron Lett 2009, 5, 5649.
[66] Rao, M. S.; Chhikara, B. S.; Tiwari, R.; Shirazi, A. N.; Parang, K.; Kumar, A. A. Chem Biol Interact 2012, 2, 362.
[67] Wang, Y.; Ye, H.; Zuo, G.; Luo, J. J Mol Liq 2015, 212, 418.
[68] Chen, L.; Huang, X. J.; Li, Y. Q.; Zhou, M. Y.; Zheng, W. J. Monatshefte für Chemie-Chemical Monthly 2009, 140, 45.
[69] Tahmassebi, D.; Bryson, J. A.; Binz, S. I. Synth Commun 2011, 41, 2701.

SUPPORTING INFORMATION

Additional supporting information may be found online in the Supporting Information section at the end of the article.